POLITECNICO DI TORINO
Repository ISTITUZIONALE

Majorana-like localized spin density without bound states in topologically trivial spin-orbit coupled nanowires

Original
Majorana-like localized spin density without bound states in topologically trivial spin-orbit coupled nanowires / Rossi, L., Dolcini, F., Rossi, F.. - In: PHYSICAL REVIEW. B. - ISSN 2469-9969. - STAMPA. - 101:19(2020), p. 195421. [10.1103/PhysRevB.101.195421]

Availability:
This version is available at: 11583/2837482 since: 2020-06-26T15:30:05Z

Publisher:
American Physical Society

Published
DOI:10.1103/PhysRevB.101.195421

Terms of use:

This article is made available under terms and conditions as specified in the corresponding bibliographic description in the repository

Publisher copyright

(Article begins on next page)

26 November 2026

Majorana-like localized spin density without bound states in topologically trivial spin-orbit coupled nanowires

Lorenzo Rossi,* Fabrizio Dolcini, and Fausto Rossi
Dipartimento di Scienza Applicata e Tecnologia, Politecnico di Torino, 10129 Torino, Italy

(Received 20 February 2020; accepted 28 April 2020; published 13 May 2020)

In the topological phase of spin-orbit coupled nanowires Majorana bound states are known to localize at the nanowire edges and to exhibit a spin density orthogonal to both the magnetic field and the spin-orbit field. By investigating a nanowire exposed to a uniform magnetic field with an interface between regions with different spin-orbit couplings, we find that the orthogonal spin density is pinned at the interface even when both interface sides are in the topologically trivial phase, and even when no bound state is present at all. A trivial bound state may additionally appear at the interface, especially if the spin-orbit coupling takes opposite signs across the interface. However, it can be destroyed by a smoothening of the spin-orbit profile or by a magnetic field component parallel to the spin-orbit field. In contrast, the orthogonal spin density persists in various and realistic parameter ranges. We also show that, while the measurement of bulk equilibrium spin currents has been elusive so far, such robust orthogonal spin density peak may provide a way to detect spin current variations across interfaces.

DOI: 10.1103/PhysRevB.101.195421

I. INTRODUCTION

Topological materials have been under the spotlight of experimental and theoretical research for years by now, due to their relevance in terms of fundamental physics and their broad spectrum of applications, from spintronics to quantum computing [1–3]. One of the most remarkable features of a topological phase is that edge states localize at the interface with a topologically trivial phase. Indeed several theoretical analysis have shown that such interface states emerge at the boundaries of topological insulators (TIs), like the one-dimensional Su-Schrieffer-Heeger model for polyacetylene [4–6] or the two-dimensional quantum spin Hall systems [7–11]. Similarly, as first predicted by Kitaev [12], at the edges of topological superconductors [13–15], realized in proximized nanowires (NWs) with Rashba spin-orbit coupling (RSOC) [16,17], in ferromagnetic atomic chains deposited on a superconductor [18], or in two-dimensional TIs proximized by superconductors and magnets [19–21], Majorana quasiparticles (MQPs) appear. These exotic quasiparticles, which are equal to their antiparticles, are currently considered a promising platform for quantum computing in view of their nontrivial braiding properties and their robustness to charge decoherence effects [22–26].

While in theoretical models a topological phase is characterized by a well specified range of parameters in the Hamiltonian, when it comes to finding an experimental evidence of such phase in a given material, the difficult question is "how to distinguish signatures of a topological from a trivial bound state?" As a general criterion, a topological bound state is stable to perturbations that do not close the gap of the topological phase, while a trivial bound state is not. However, because in a given experimental setup the actual parameter range characterizing the topological phase is not known *a priori* and/or may be relatively narrow, the search for such stable signatures is in general not a trivial task. For instance, although it is by now commonly accepted that MQPs exist in RSOC nanowires [27–34], the early observations of a zero-bias conductance peak stable to magnetic field and Fermi energy variations were cautiously claimed to be *compatible* with the existence of MQPs. The remark that such a scenario may also be caused by Kondo effect [35], disorder [36,37], or inhomogeneities [38] has recently spurred further investigations, which pointed out that in the topological phase also trivial bound states may be present [38–44]. Furthermore, a quite recent analysis [45], carried out on a nanowire with homogeneous RSOC and with inhomogeneous magnetic field, showed that at the interface between two magnetic domains with opposite magnetization directions, bound states appear that are unrelated to the Jackiw-Rebbi topological states.

A more clear evidence of topological bound states requires a spatially resolved analysis. This was done, for instance, in ferromagnetic atomic chains deposited on a superconductor [46], where the combined use of spatially resolved spectroscopic and spin-polarized measurements showed that zero-bias conductance peaks are due to states localized at the ends of the chain. Yet, the smoking gun enabling one to identify such states with MQPs is their disappearance in the normal state, when superconductivity is suppressed. As far as NWs are concerned, it has been pointed out that MQPs in the topological phase exhibit an *orthogonal* spin density, i.e., a component perpendicular to both the magnetic and spin-orbit fields, localized at the NW ends [47–49]. In order to identify a topological phase in a given system, it is thus particularly important to understand whether and when the

*lorenzo.rossi@polito.it

 ©2020 American Physical Society

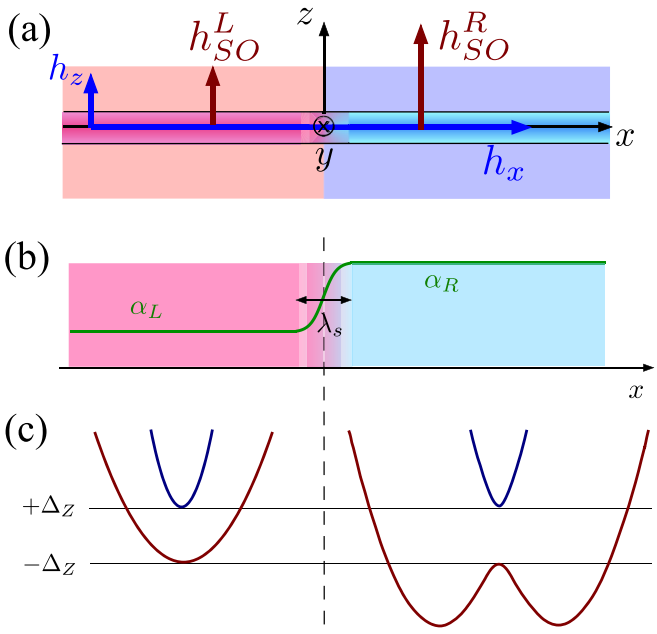

FIG. 1. (a) Top view of a Rashba nanowire deposited on a substrate: the Rashba effective magnetic field $h^{\rm SO}$ is directed along z, whereas an actual magnetic field, externally applied in the substrate plane, has components in the x-z substrate plane. The NW contains an interface between two regions with different RSOC values. (b) The spatial profile of the RSOC across the interface of the NW, ranging from the bulk values α_L to α_R over a smoothening length scale λ_s. (c) Examples of electronic bands related to the bulks of the two interface sides, the left-hand side in the Zeeman dominated regime, and the right-hand side in the Rashba-dominated regime.

topologically trivial phase may exhibit observables that are spatially localized at the interfaces and that may mistakenly be interpreted as a topological signature. So far, this aspect has been analyzed far less than the topological bound states.

This paper is meant to bridge this gap. Specifically, we consider the case of a RSOC NW exposed to a uniform magnetic field, and we analyze the spatial profile of charge and spin densities at the interface between two regions with different values of RSOC, as sketched in Fig. 1(a). Such types of interfaces emerge quite naturally in any realistic setup, since metallic electrodes or gates are typically deposited on top of a portion of the NW, thereby altering the underneath structure inversion asymmetry characterizing the very RSOC. Furthermore, the recent advances in various gating techniques, including gate-all-around approaches, allow a large tunability of the RSOC constant, possibly even changing the RSOC sign [50–57].

Importantly, on both sides of the interface, the NW that we consider is in the *topologically trivial phase*, since no superconducting coupling is included. Furthermore, as the gap depends only on the strength of the magnetic field, it never closes at the interface, since the magnetic field is assumed to be *uniform*. Thus, under these conditions the existence of bound states of topological origin is ruled out *a priori*.

Our analysis unveils various noteworthy aspects. In the first instance, a bound state may appear at the interface. Importantly such bound state, while being not topological, is *not* a customary interface state merely arising from the inhomogeneity of the RSOC. Indeed it can only exist if an external magnetic field is applied orthogonally to the RSOC field direction, and if its intensity fulfills specific conditions with respect to the two spin-orbit energies characterizing the two NW regions. The conditions of existence and the robustness of the bound state are analyzed in details in terms of different values of RSOC across the interface, including the smoothening length characterizing the crossover between these two values and the presence of a magnetic field component parallel to the RSOC field direction.

Second, we find for realistic values of chemical potential and temperature that the orthogonal spin density exhibits a peak pinned at the interface. Despite the NW is in the topologically trivial phase, such a peak is relatively robust to other parameter variations. In fact, we show that it persists even when the bound state is absent, indicating that in such a case also the continuum states locally modify their spin texture to maintain such effect.

Furthermore, by considering the case of two interfaces, we show that the peaks of the orthogonal spin density are opposite at the two ends of the inner NW region, similarly to what occurs for MQPs in the topological phase.

These results imply that a localized orthogonal spin density can neither be taken as a unique signature of a MQP nor of a topologically trivial bound state. However, we argue that it can represent a useful way to indirectly detect spin current differences. Indeed, while the detection of a bulk equilibrium spin current, which emerges in a homogeneous NW from the correlations between spin and velocity induced by the magnetic and spin-orbit fields [58], has been elusive so far, any *variation* of equilibrium spin current occurring at the interface is precisely related to the orthogonal spin-density peak predicted here.

The paper is organized as follows. In Sec. II we introduce the model and describe the involved energy scales. In Sec. III we present the results concerning the bound state, discussing first the case of a sharp RSOC interface profile in the presence of a magnetic field applied along the NW axis. Then we analyze the more realistic case of a finite smoothening length in the profile, and address the effect of a magnetic field component parallel to the spin-orbit field direction. In Sec. IV we investigate the spatial profile of the charge and spin densities, and analyze specifically the bound state contribution to them. In Sec. V we discuss the interpretation of our main results, we include the case of two interfaces and we propose some possible experimental realizations. Finally, in Sec. VI we draw our conclusions.

II. THE MODEL FOR A SOC INTERFACE

A. Nanowire Hamiltonian

Let x denote the longitudinal axis of a NW deposited on a substrate. The NW is characterized by a RSOC, which is assumed to take two different values α_L and α_R on the left and on the right side of an interface, respectively [see Figs. 1(a) and 1(b)]. This inhomogeneity in the RSOC profile $\alpha(x)$ may result, e.g., from the presence of a gate covering only one portion of the NW, or by two different gate voltage values

applied to top/bottom gates or to the substrate. The crossover between α_L and α_R occurs over a smoothening length λ_s. Denoting by z the direction of the spin-orbit field $\mathbf{h}^{\rm SO}$, i.e., the effective "magnetic" field generated by the RSOC [see Fig. 1(a)], the NW Hamiltonian is

$$\hat{\mathcal{H}} = \int \hat{\Psi}^\dagger(x)\, H(x)\, \hat{\Psi}(x)\, dx, \tag{1}$$

where

$$H(x) = \frac{p_x^2}{2m^*}\sigma_0 - \frac{\{\alpha(x),\, p_x\}}{2\hbar}\sigma_z - \mathbf{h}\cdot\boldsymbol{\sigma}. \tag{2}$$

Here $\hat{\Psi}(x) = (\hat{\Psi}_\uparrow(x), \hat{\Psi}_\downarrow(x))^T$ is the electron spinor field, with $\uparrow, \downarrow$ corresponding to spin projections along z, $p_x = -i\hbar\partial_x$ is the momentum operator, m^* is the NW effective mass, σ_0 is the 2×2 identity matrix, and $\boldsymbol{\sigma} = (\sigma_x, \sigma_y, \sigma_z)$ are the Pauli matrices. For definiteness, we take the location of the interface at $x = 0$. The anticommutator in Eq. (2) is necessary since p_x does not commute with the inhomogeneous RSOC $\alpha(x)$ [59,60]. The last term in Eq. (2), where $\mathbf{h} = g\mu_B\mathbf{B}/2$, describes the Zeeman coupling with an external uniform magnetic field $\mathbf{B} = (B_x, 0, B_z)$ applied in the substrate plane, with μ_B denoting the Bohr magneton and g the NW Landé factor. It is useful to decompose the magnetic gap energy vector as $\mathbf{h} = h_x\mathbf{i}_x + h_z\mathbf{i}_z$, where h_x and h_z denote the components parallel and perpendicular to the nanowire axis x, i.e., perpendicular and parallel to the Rashba spin-orbit field direction z, respectively [see Fig. 1(a)]. Although for most of our analysis we shall focus on the case of the magnetic field directed along the nanowire axis x, we shall also discuss the effects of the component h_z parallel to $\mathbf{h}^{\rm SO}$.

B. Energy scales

In order to describe the results about the inhomogeneous RSOC profile at the interface, it is first worth pointing out the energy scales involved in the problem.

1. The homogeneous NW

Let us start by briefly summarizing the case of a homogeneous profile $\alpha(x) \equiv \alpha$ in Eq. (2), for an infinitely long NW. In such a case the Hamiltonian (2) commutes with p_x, and the spectrum reads [58–60]

$$E_\pm(k) = \varepsilon_k^0 \pm \sqrt{h_x^2 + (\alpha k + h_z)^2}, \tag{3}$$

where $\varepsilon_k^0 = \hbar^2k^2/2m^*$ is the customary parabolic spectrum in the absence of RSOC and magnetic field. The spectrum (3) describes two bands separated by a minimal gap $2\Delta_Z$, where the quantity

$$\Delta_Z = |h_x| \tag{4}$$

shall be henceforth called the magnetic gap energy. Moreover, the RSOC α identifies the spin-orbit wave vector $k_{\rm SO} = m^*|\alpha|/\hbar^2$, which characterizes, in the absence of external magnetic field, the two degenerate minima $E(\pm k_{\rm SO}) = -E_{\rm SO}$ of the spectrum, where

$$E_{\rm SO} = \frac{m^*\alpha^2}{2\hbar^2} = \frac{\hbar^2 k_{\rm SO}^2}{2m^*} \tag{5}$$

is called the spin-orbit energy.

In the case $h_z = 0$ the magnetic field is directed along x, i.e., orthogonal to the RSOC field, the spectrum (3) is symmetric $E_\pm(-k) = E_\pm(+k)$. Two regimes can be identified:

(a) In the *Zeeman-dominated regime* ($\Delta_Z > 2E_{\rm SO}$) both bands have a minimum at $k = 0$, which takes values $E_\pm^{\rm min} = \pm\Delta_Z$, respectively.

(b) In the *Rashba-dominated regime* ($\Delta_Z < 2E_{\rm SO}$), the upper band still has a minimum $E_+^{\rm min} = +\Delta_Z$ at $k = 0$, while the lower band acquires two lower and degenerate minima $E_-^{\rm min} = -E_{\rm SO} - \Delta_Z^2/4E_{SO}$ occurring at $k = \pm k^{\rm min}$, with

$$k^{\rm min} = k_{\rm SO}\sqrt{1 - \Delta_Z^2/4E_{\rm SO}^2}. \tag{6}$$

When a component $h_z \neq 0$ parallel to the RSOC field is also present, the minimal gap $2\Delta_Z$ between the two bands occurs at $k = -h_z/\alpha$ and the spectrum is no longer symmetric $E_\pm(-k) \neq E_\pm(+k)$.

The eigenfunctions related to the spectrum (3) read

$$\psi_{k\pm}(x) = w_{k\pm}\exp[ikx]/\sqrt{\Omega}, \tag{7}$$

with Ω denoting the system length. They describe plane waves with spinors

$$w_{k-} = \begin{pmatrix}\cos\frac{\theta_k}{2}\\ \sin\frac{\theta_k}{2}\end{pmatrix}, \quad w_{k+} = \begin{pmatrix}-\sin\frac{\theta_k}{2}\\ \cos\frac{\theta_k}{2}\end{pmatrix}, \tag{8}$$

whose spin orientation $\mathbf{n}(k) \equiv (\sin\theta_k\,, 0\,, \cos\theta_k)$ lies on the x-z substrate plane and forms with the z axis an angle $\theta_k \in [-\pi\,, \pi\,]$. The latter, defined through

$$\begin{aligned}\cos\theta_k &= \frac{\alpha k + h_z}{\sqrt{(\alpha k + h_z)^2 + h_x^2}},\\ \sin\theta_k &= \frac{h_x}{\sqrt{(\alpha k + h_z)^2 + h_x^2}},\end{aligned} \tag{9}$$

depends on the wave vector k, the magnetic field, and the RSOC α. In particular, it is worth recalling that in the case of a magnetic field along the NW axis ($h_z = 0$) and in the deep Rashba-dominated regime ($\Delta_Z \ll 2E_{\rm SO}$) the states with energy inside the magnetic gap mimic the helical edge states of the quantum spin Hall effect. Indeed their spin orientation, determined mainly by the RSOC, is opposite for right- and left-moving electrons, whose helicity is determined by the *sign* of the RSOC α. This is precisely the most suitable regime for the topological phase to be induced by an additional s-wave superconducting coupling [16,17,61,62].

2. The NW with a RSOC interface

When an interface separates two portions of a NW characterized by two different values α_L and α_R of RSOC [see Fig. 1(b)], the momentum p_x does not commute with the Hamiltonian characterized by an inhomogeneous $\alpha(x)$ profile, and the spectrum cannot be labeled by a wave vector k. Before attacking the inhomogeneous problem in the next section, it is worth identifying the energy scales and the possible scenarios one can expect in the interface problem from a preliminary analysis of the bulks of the two regions across the RSOC interface. To begin with, the two bulk values α_L and α_R of

the two NW regions lead to two spin-orbit energies (5)

$$E_{\mathrm{SO},\nu} = \frac{m^*\alpha_\nu^2}{2\hbar^2}, \quad \nu = R/L. \tag{10}$$

Without loss of generality, we shall choose the RSOC with higher magnitude $|\alpha|$ on the right-hand side, and we can set it to a positive value $\alpha_R > 0$, whereas the RSOC on the left-hand side is allowed to take any value in the range $-\alpha_R \leqslant \alpha_L \leqslant \alpha_R$ [63]. Correspondingly, one has $E_{\mathrm{SO},L} \leqslant E_{\mathrm{SO},R}$. The fact that the magnetic field is uniform has important consequences, which are easily illustrated in the case $h_z = 0$: First, in the bulk of each region the gap between the bands is always given by $2\Delta_Z$, regardless of the regime (Rashba or Zeeman dominated) of each interface side. Second, the overall minimum of the two energy band bottoms is determined by the band bottom of the side with higher spin-orbit energy, i.e., the right-hand side, and is thus given by

$$E_{\mathrm{band}}^{\mathrm{min}} = \begin{cases} -\Delta_Z, & \text{if } \Delta_Z > 2E_{\mathrm{SO},R}, \\ -E_{\mathrm{SO},R}\left(1 + \frac{\Delta_Z^2}{4E_{\mathrm{SO},R}^2}\right), & \text{if } \Delta_Z < 2E_{\mathrm{SO},R}. \end{cases} \tag{11}$$

With these notations, if the right side is in the Zeeman-dominated regime, so is the left-hand side, whereas if the right side is in the Rashba-dominated regime the left-hand side can be either in the Rashba- or in the Zeeman-dominated regime. There can thus be only three possible regime combinations: (i) $E_{\mathrm{SO},L} \leqslant E_{\mathrm{SO},R} \leqslant \Delta_Z/2$, where both sides are Zeeman dominated; (ii) $\Delta_Z/2 \leqslant E_{\mathrm{SO},L} \leqslant E_{\mathrm{SO},R}$, where both sides are Rashba dominated; and (iii) $E_{\mathrm{SO},L} \leqslant \Delta_Z/2 \leqslant E_{\mathrm{SO},R}$, where the left side is Zeeman dominated while the right side is Rashba dominated. The bands of the latter case are illustrated as an example in Fig. 1(c).

III. BOUND STATE AND ITS STABILITY

In this section we focus on the inhomogeneous interface problem. By diagonalizing the inhomogeneous Hamiltonian, with methods to be described here below, we find that its spectrum always exhibits a continuum branch, whose bottom $E_{\mathrm{cont}}^{\mathrm{min}}$ coincides with the minimal band energy obtained in Eq. (11) from the comparison of bare bulk spectra. However, for some parameter range (see below), the spectrum also displays an additional eigenvalue E_{bs}, lying *below* the continuum spectrum $E_{\mathrm{cont}}^{\mathrm{min}}$. The related eigenfunction exhibits an evanescent behavior for $|x| \to \infty$. When such bound state exists, we define its positive "binding energy" as

$$E_b = E_{\mathrm{cont}}^{\mathrm{min}} - E_{\mathrm{bs}} > 0. \tag{12}$$

Here below we now analyze the conditions for its existence.

A. The case of a sharp interface

Let us start by analyzing the existence of the bound state in the case of a sharp interface, where the smoothening length $\lambda_s \to 0$ vanishes and the profile can be assumed as

$$\alpha(x) = \alpha_L\theta(-x) + \alpha_R\,\theta(x), \tag{13}$$

with θ denoting the Heaviside function. In this case the eigenfunctions of the inhomogeneous problem can be obtained analytically by combining the eigenstates (7) of the homogeneous problem in each side and by matching them appropriately at the interface. In particular, since bound states are eigenstates with evanescent wave function for $|x| \to \infty$, they are obtained requiring that the wave vector k acquires an imaginary part. Details of such calculation can be found in Appendix A.

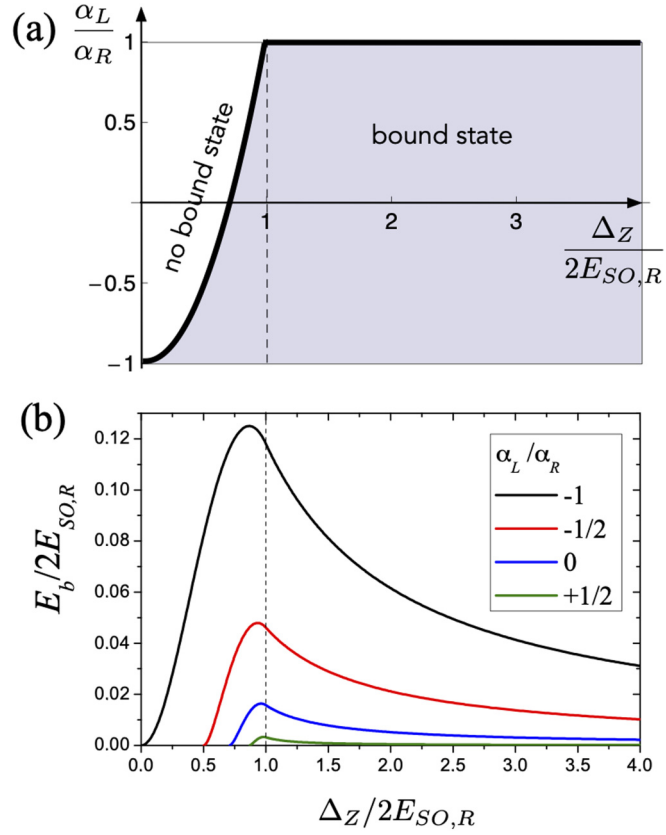

FIG. 2. The case of a sharp profile interface Eq. (13). (a) The phase diagram for the existence of the bound state is shown as a function of the magnetic gap energy (in units of twice the maximal spin-orbit energy $2E_{\mathrm{SO},R}$) and of the ratio between the two RSOC values across the interface. The thick black line identifies the transition curve, where the binding energy vanishes. The vertical thin dashed line indicates the crossover value from the Rashba-dominated to the Zeeman-dominated regime for the right side of the interface. (b) The binding energy E_b of the bound state as a function of $\Delta_Z/2E_{\mathrm{SO},R}$ for four different values of the RSOC ratio across the interface.

By keeping one side of the junction as a reference, e.g., the right-hand side where the bulk spin-orbit energy is maximal, the problem can be formulated in terms of dimensionless parameters, namely the RSOC ratio $\alpha_L/\alpha_R \in [-1\,,\,1]$ and the energy ratios $E_b/E_{\mathrm{SO},R}$ and $\mathbf{h}/E_{\mathrm{SO},R}$ to the maximal spin-orbit energy $E_{\mathrm{SO},R}$. We shall focus here below on the case where the applied magnetic field is directed only along the nanowire axis x, $\mathbf{h} = h_x\mathbf{i}_x$, i.e., orthogonally to the Rashba spin-orbit field, while the effects of a parallel magnetic field component h_z will be discussed later.

The results are presented in Fig. 2. In particular, Fig. 2(a) displays the phase diagram of the existence of the bound state. For a sufficiently strong magnetic field, $\Delta_Z > 2E_{\mathrm{SO},R}$, i.e., when both NW sides are in the Zeeman-dominated regime,

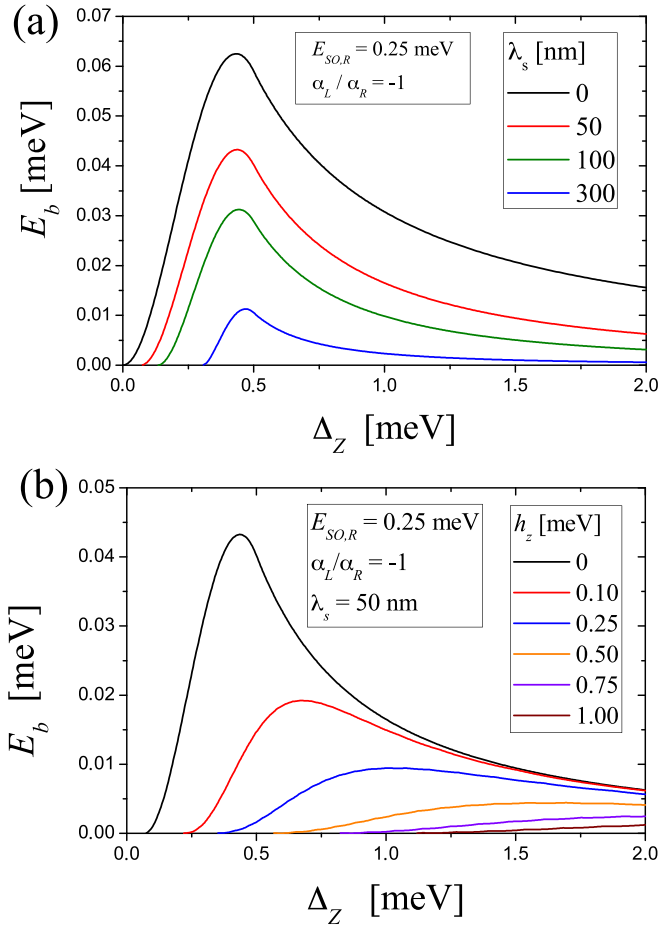

FIG. 3. The binding energy as a function of the magnetic gap energy, for an interface with $\alpha_L = -\alpha_R$, with $E_{\mathrm{SO},R} = E_{\mathrm{SO},L} = 0.25$ meV. (a) The effects of a smoothening length. (b) Effects of a magnetic field component h_z parallel to the spin-orbit field on the binding energy, for a fixed smoothening length $\lambda_s = 50$ nm.

the bound state always exists, while for $\Delta_Z < 2E_{\mathrm{SO},R}$, where the NW right side is in the Rashba-dominated regime, the bound state may or may not exist. In particular, for $\Delta_Z = 0$ (no external magnetic field), the bound state never exists, regardless of the ratio of the two RSOC values across the interface. This shows that the bound state, although it has no topological origin, it is not an intrinsic interface state like the ones occurring at a customary semiconductor interface. The thick black in Fig. 3(a) denotes the transition curve for the existence of the bound state, and corresponds to the vanishing of the binding energy $E_b = 0$. In particular, the parabolic curve for $\Delta_Z/2E_{\mathrm{SO},R} < 1$ is described by the equation

$$\frac{\Delta_Z^\star}{2E_{\mathrm{SO},R}} = \sqrt{\frac{1+\alpha_L/\alpha_R}{2}}, \tag{14}$$

while the upper horizontal line corresponds to the homogeneous NW in the Zeeman-dominated regime, where the bound state does not exist, as is obvious to expect. Then, Fig. 2(b) shows, for four different values of the ratio α_L/α_R, the behavior of the binding energy E_b as a function of the ratio $\Delta_Z/2E_{\mathrm{SO},R}$. Several features are noteworthy.

First, in all cases the binding energy exhibits a nonmonotonic behavior as a function of the magnetic gap energy, with a maximum $E_b^{\max}$ occurring for a magnetic gap energy slightly below the transition value $\Delta_Z = 2E_{\mathrm{SO},R}$ between the Rashba- and Zeeman-dominated regime of the right-hand side, highlighted by the vertical dashed line as a guide to the eye.

Second, the bound state energy strongly depends on the ratio α_L/α_R of the two RSOC values, and is typically much higher when the RSOC changes sign across the interface. In particular, the optimal condition for the existence of the bound state is $\alpha_L/\alpha_R = -1$, i.e., when the RSOC takes *equal and opposite* values of two sides: In this situation not only the bound state always exists, its binding energy is also higher than any other case. For these reasons, we shall henceforth term such case the "optimal configuration." In particular, it can be shown that, for weak applied field ($\Delta_Z \ll 2E_{\mathrm{SO},R}$), the binding energy of the optimal configuration behaves as $E_b \simeq \Delta_Z^2/4E_{\mathrm{SO},R}$, while for strong field ($\Delta_Z \gg 2E_{\mathrm{SO},R}$), one finds $E_b \simeq E_{\mathrm{SO},R}^2/2\Delta_Z$.

Third, for all other cases ($-1 < \alpha_L/\alpha_R < 1$) the bound state exists only if the magnetic gap energy overcomes a minimal threshold value, which precisely corresponds to the transition curve of Fig. 2(a) described by Eq. (14). The threshold of the magnetic gap energy increases as the RSOC ratio α_L/α_R increases from the negative value -1 to the value $+1$, corresponding to the homogeneous case. Furthermore, the following "rule of thumb" can be inferred: when the band bottoms of the two interface sides are equal, the bound state certainly exists. Indeed a close inspection of Fig. 2 shows that this certainly occurs in these two situations: (i) when $\Delta_Z/2E_{\mathrm{SO},R} > 1$, i.e., when both sides are in the Zeeman-dominated regime and their band bottoms are both equal to $-\Delta_Z$; and (ii) when $\alpha_L = -\alpha_R$, i.e., when the two spin-orbit energies (10) are equal, both sides are in the same regime (Rashba or Zeeman dominated) and thus have the same band bottoms. In all other cases the existence of the bound state depends on the specific energy ratios.

Finally, even when the bound state exists, its binding energy can be quite small. For instance, the maximal binding energy in the case where $\alpha_L/\alpha_R = 1/2$ is about 25 times smaller than the maximal value in the optimal case $\alpha_L/\alpha_R = -1$. Similarly, even in the regime $\Delta_Z/2E_{\mathrm{SO},R} > 1$ the binding energy decreases with increasing magnetic field.

B. Effects of smoothening length

In any realistic system the crossover between two RSOC bulk values occurs over a finite smoothening length λ_s. To include such an effect we now assume the following profile function:

$$\alpha(x) = \frac{\alpha_R + \alpha_L}{2} + \frac{\alpha_R - \alpha_L}{2}\,\mathrm{Erf}\left(\frac{\sqrt{8}\,x}{\lambda_s}\right), \tag{15}$$

which varies from α_L to α_R up to 2% within the length scale λ_s. In Eq. (15) Erf denotes the error function. Although in the presence of such smoothened profile the model cannot be solved analytically, it can be approached by an exact numerical diagonalization of the Hamiltonian (2), with a method similar to the one introduced in Ref. [58], whose details specific

to the profile (15) are summarized in Appendix B. Instead of expressing the results in terms of dimensionless parameters, we now choose to fix the parameters to realistic setup values. For definiteness we consider the case of a InSb NW, with an effective mass $m^* = 0.015\ m_e$ and a maximal spin-orbit energy $E_{\mathrm{SO},R} = 0.25$ meV. Furthermore, in order to appreciate the effects of the smoothening length, we focus on the case of the optimal configuration $\alpha_R/\alpha_L = -1$. The results, displayed in Fig. 3(a), show the binding energy as a function of the magnetic gap energy Δ_Z for four different values of the smoothening length. As one can see, while for the ideal case $\lambda_s \to 0$ (sharp profile) the bound state always exists, for any finite smoothening length the bound state only appears above a threshold value for the Zeeman field. For sufficiently strong applied magnetic field (Zeeman-dominated regime) the bound state always exists. However, the binding energy exhibits an overall suppression for increasing λ_s. These effects can be understood be realizing that a crossover from $-\alpha_R$ to α_R in the RSOC profile occurring over a finite smoothening length can, to a first approximation, be considered as a stairlike sequence of smaller sharp α steps. As the analysis carried out above on the sharp profile indicates (see Fig. 2), in the case of a nonoptimal jump $\alpha_L > -\alpha_R$, a threshold value for Δ_Z does exist and the binding energy is reduced. In summary, a finite smoothening length λ_s broadens the white portion of the sharp-profile phase diagram Fig. 2(a) where the bound state does not exist, and suppresses the binding energy.

C. Effects of a parallel field component

So far we have analyzed cases where the magnetic field h_x is directed along the NW. Here we want to discuss the effect of a magnetic field component h_z parallel to the spin-orbit field. We first point out that, for $h_z \neq 0$ and $h_x = 0$, i.e., for a magnetic field directed purely along the spin-orbit field direction z, the eigenvalue problem for the Hamiltonian (2) completely decouples in the two spin-$\uparrow$ and spin-$\downarrow$ components, and it can be shown that the bound state does not exist (see Appendix A). The orthogonal field component h_x is thus a necessary, though not sufficient, condition for the bound state to exist. One can then analyze how the parallel field component h_z modifies the existence of the bound state, for a fixed value of $h_x \neq 0$. To this purpose, we focus again on a InSb NW, with an optimal configuration $\alpha_R = -\alpha_L > 0$, and we take a realistic smoothening length $\lambda_s = 50$ nm. The result, displayed in Fig. 3(b), shows that the presence of an additional parallel field component h_z modifies the dependence of the binding energy E_b as a function of the magnetic gap energy Δ_Z, especially by increasing the threshold value $\Delta_Z^\star$ at which the bound state starts to exist. Similarly to the case of the smoothening length, the binding energy values are quite reduced as compared to the case $h_z = 0$.

IV. CHARGE AND SPIN DENSITY SPATIAL PROFILES

In the previous section we have discussed the existence and the robustness of the bound state, which is a spectral feature. Here we wish to analyze spatial behavior of physical observables, namely the charge and spin densities, described by the operators

$$\hat{n}(x) = e\,\hat{\Psi}^\dagger(x)\,\hat{\Psi}(x), \tag{16}$$

$$\hat{\mathbf{S}}(x) = \frac{\hbar}{2}\,\hat{\Psi}^\dagger(x)\,\boldsymbol{\sigma}\,\hat{\Psi}(x), \tag{17}$$

respectively, where e denotes the electron charge. The presence of the interface makes the NW an inhomogeneous system, and we aim to investigate the spatial profile of the equilibrium expectation values

$$\rho(x) \equiv \frac{1}{e}\langle\hat{n}(x)\rangle_\circ, \tag{18}$$

$$\mathbf{s}(x) \equiv \frac{2}{\hbar}\langle\hat{\mathbf{S}}(x)\rangle_\circ, \tag{19}$$

with a particular focus on their behavior near the interface. Details about the computation of such expectation values can be found in Appendix B. Before presenting our results, a few general comments are in order.

Chemical potential and temperature. The equilibrium distribution determining the expectation values (18) and (19) is characterized by a well defined value of chemical potential μ and temperature T. As pointed out above, the whole spectrum of the inhomogeneous Hamiltonian (2), which we obtain by an exact numerical diagonalization, consists of a continuum spectrum, related to extended propagating states, and possibly (if present) a bound state, energetically lying below the continuum and corresponding to a state localized at the interface. At equilibrium, and ideally at zero temperature, all states (localized or extended) with energy up to the chemical potential μ are filled up, and contribute to determine the equilibrium expectation values $\rho(x)$ and $\mathbf{s}(x)$, while at finite temperature the Fermi function is smeared over a range $k_B T$ around the chemical potential. We shall choose for T and μ realistic values of low-temperature experimental setups involving NWs, namely $T = 250$ mK and $\mu = 0$, corresponding to the energy value in the middle of the magnetic gap [see Fig. 1(c)]. This is the situation, for instance, where the Fermi energy states of a NW in the Rashba-dominated regime mimic the helical states of a quantum spin Hall system.

Orthogonal spin density. Concerning the spin density $\mathbf{s}(x)$ in Eq. (19), we shall specifically focus on s_y component, which we shall refer to as the *orthogonal spin density*, since it is orthogonal to the x-z plane identified by the applied magnetic field and the spin-orbit field. The interest in analyzing the profile of $s_y(x)$ stems from a comparison with the topological phase. Indeed it has been predicted [47–49] that the MQPs appearing at the ends of a proximitized NW in the topological phase, are precisely characterized by a nonvanishing expectation value s_y. However, we shall show here below that such orthogonal spin density already appears in the NW interface problem, where the NW is certainly in the topologically trivial phase, so that it cannot be considered as a signature of a MQP.

Full vs bound state contribution. Bound states and orthogonal spin density s_y share two properties. First, both can only exist at an interface, i.e., in the presence of inhomogeneities. Indeed, in the bulk of a homogeneous NW, s_y vanishes since the spin orientation of each electron lies in the x-z plane [see

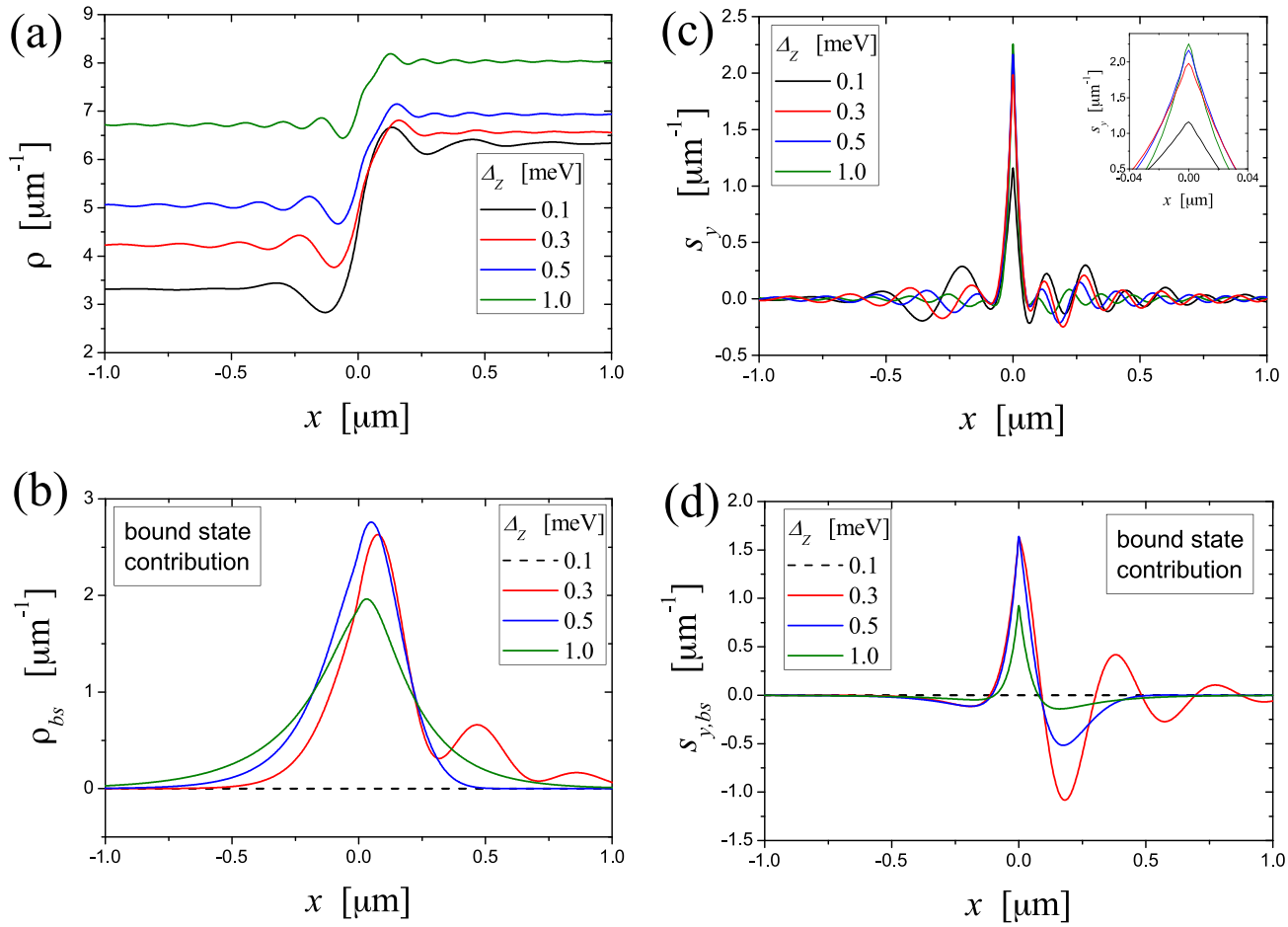

FIG. 4. Spatial profiles of charge density and orthogonal spin density for a sharp interface profile Eq. (13) with $\alpha_L/\alpha_R = -1/2$ and $E_{\mathrm{SO},R} = 0.25$ meV. The four different curves in each panel refer to four different values of the magnetic gap energy $\Delta_Z = (0.1, 0.3, 0.5, 1.0)$ meV. (a) The actual equilibrium density profile $\rho(x)$ [see Eq. (18)]. (b) The bound state contribution $\rho_{bs}(x)$ to the density $\rho(x)$. For $\Delta_Z = 0.1$ meV the bound state does not exist and yields a vanishing contribution (black dashed curve). (c) The full orthogonal spin density s_y Eq. (19) (with the inset magnifying the peaks) while (d) describes the related bound state contribution $s_{y,\mathrm{bs}}$.

Eqs. (8) and (9)]. Second, just like the bound state, s_y may only exist if both a magnetic field component h_x and the spin-orbit field are present. Indeed if $h_x = 0$ (or $\alpha = 0$) the electron spin is directed, along z (or x) for all states. In view of such common features, one is naively tempted to conclude that an orthogonal spin density is necessarily ascribed to the presence of the bound state. However, this is not the case. To this purpose, we shall illustrate below two types of spatial profiles. First, we shall show the actual equilibrium values $\rho(x)$ and $s_y(x)$ [see Eqs. (18) and (19)], which can be referred to as the "full" density and orthogonal spin density profiles, as they result from contributions of all states, with the customary weight given by the Fermi function. In particular, since we focus on the low temperature regime, the latter essentially amounts to the contribution of all states occupied up to the chemical potential μ. Then we shall also provide the profiles $\rho_{\mathrm{bs}}(x)$ and $s_{y,\mathrm{bs}}(x)$ describing the contribution to $\rho(x)$ and $s_y(x)$ due to the localized bound state only (see Appendix B for details).

This distinction enables us to show that an orthogonal spin density peak, besides being no evidence for a MQP, may also not originate from any bound state.

A. The case of a sharp profile with an orthogonal magnetic field

Let us start our analysis from the case of a sharp profile interface and a magnetic field applied along the NW axis. As an illustrative example, we consider an interface with $\alpha_L/\alpha_R = -1/2$, which implies $E_{\mathrm{SO},L} = E_{\mathrm{SO},R}/4$ [see Eq. (10)], and we choose a value of $E_{\mathrm{SO},R} = 0.25$ meV for the maximal spin-orbit energy.

Figure 4(a) shows the full equilibrium density Eq. (18), for four different values of the magnetic gap energy Δ_Z of the applied magnetic field h_x. Its spatial profile $\rho(x)$ exhibits a crossover at the interface $x = 0$ between two different bulk density values. The density increases towards the right-hand side, namely the region with higher spin-orbit energy, whose band bottom is lower than on the left-hand side with lower spin-orbit energy, as observed above in Sec. IIB2. This indicates that a higher spin-orbit energy has a similar effect on the density as a lower gate voltage bias.

In Fig. 4(b) we have singled out the contribution ρ_{bs} due to the bound state only. Differently from $\rho(x)$, the profile of $\rho_{\mathrm{bs}}(x)$ is localized only around the interface and is dramatically sensitive to the value of Δ_Z. Indeed, as can be deduced

from Eq. (14), the minimal threshold for the appearance of the bound state is, for the chosen parameters, $\Delta_Z^\star = E_{\mathrm{SO},R} = 0.25$ meV. For values $\Delta_Z > \Delta_Z^\star$ [red, blue, and green curves in Fig. 4(b)], where the bound state exists, a comparison of the height of the peak of ρ_{bs} with the profile of the full ρ [Fig. 4(a)] suggests that the increase of ρ across the interface is mainly due to the presence of the bound state. However, for a magnetic gap energy $\Delta_Z < \Delta_Z^\star$ [black dashed curve in Fig. 4(b)], ρ_{bs} is vanishing because the bound state is absent. Note the striking difference from the behavior of the full $\rho(x)$ across the interface [Fig. 4(a)], which is instead qualitatively very similar for all values of the magnetic gap energy Δ_Z. In conclusion, the increase of the profile of ρ at the interface is not necessarily ascribed to a bound state. This sounds reasonable, since the electron density is a bulk property receiving contributions from all states up to the chemical potential, and the bound state is just one of such contributions. The same reasoning holds for the s_x component of the spin density [see Eq. (19)], which is also a bulk quantity, due to the applied magnetic field h_x.

Let us now turn to consider the spin density s_y. Differently from ρ and from s_x, the orthogonal spin density s_y is vanishing in the bulk of a homogeneous NW, as observed above. Thus, s_y can only exist (if it does) in the presence of inhomogeneities, and one could naively expect that it is the hallmark of the presence of a bound state localized at the interface. The profile of the full s_y, plotted in Fig. 4(c), provides two important insights. First, a peak of the orthogonal spin density s_y does exist, even if the NW is in the topologically trivial phase, implying that it cannot be a unique signature of MQP. Second, the central peak at the interface is weakly sensitive to the values of the magnetic gap energy Δ_Z. This is in striking contrast to the behavior of the bound state contribution $s_{y,\mathrm{bs}}$, shown in Fig. 4(d), which is again strongly dependent on the magnetic field. In particular, just like the density ρ_{bs}, for weak Zeeman field $s_{y,\mathrm{bs}}$ vanishes since the bound state is absent (dashed curve), while for higher magnetic field its broadening depends on Δ_Z. These results show that a localized peak of orthogonal spin density s_y is not necessarily ascribed to the presence of a bound state, neither topological nor trivial.

Before concluding this subsection, a few further comments about Fig. 4 are in order. We observe that, while the spatial profile of the bound state density ρ_{bs} [Fig. 4(b)] is smooth, the profile of $s_{y,\mathrm{bs}}$ [Fig. 4(d)] exhibits a cusp at the interface. This difference originates from the boundary conditions induced by the sharp profile (13), which cause spin-diagonal observables like ρ and s_z to have continuous derivatives, while spin off-diagonal observables like s_x and s_y exhibit a cusp at the interface (see Appendix A). Moreover, for $\Delta_Z = 0.3$ meV, i.e., slightly above the threshold $\Delta_Z^\star = 0.25$ meV, the profiles of the bound state contributions exhibit a slowly decaying oscillations on the right-hand side, since the bound state wave function is characterized by a complex wave vector k on such side. In contrast, for $\Delta_Z = 0.5$ meV and $\Delta_Z = 1.0$ meV the wave vector is purely imaginary, and the bound state density profile has an exponential decay without oscillations. Finally, the peak of the orthogonal spin density $s_{y,\mathrm{bs}}$ has a narrower extension than the one of ρ_{bs}. This is due to the fact that, since on each interface side the bound state wave function is a linear combination of two elementary spinorial waves [see Eq. (7)], ρ_{bs} and $s_{y,\mathrm{bs}}$ are determined by different combinations of w-spinor components of the wave functions, resulting also into different weights for the space-dependent profiles.

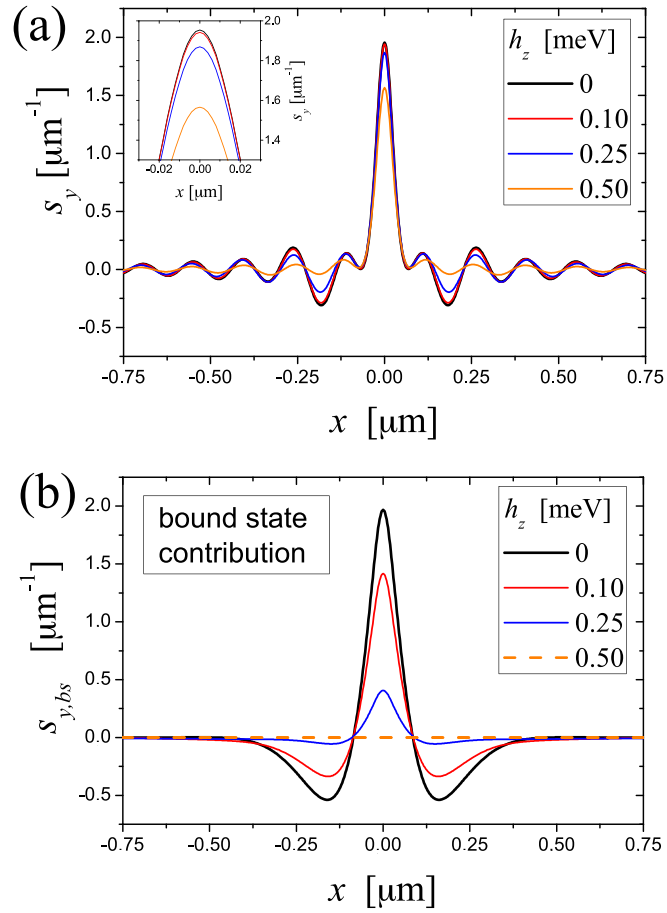

FIG. 5. Spatial profile of the orthogonal spin density for a NW interface with $\alpha_L/\alpha_R = -1$ and a smoothening length of $\lambda_s = 50$ nm. The maximal spin-orbit energy is $E_{\mathrm{SO},R} = 0.25$ meV, and the magnetic gap is $\Delta_Z = 0.50$ meV. Different curves refer to different values of the magnetic field component h_z parallel to the spin-orbit field. (a) The actual s_y due to all states, with the inset magnifying the peaks. (b) The bound state contribution to s_y.

B. Effects of a smoothened profile and parallel magnetic field on the orthogonal spin density

In the previous subsection we have shown that the peak of the orthogonal spin density is far more robust than the bound state. In order to test how general such effect is, we now extend the previous analysis including the presence of a finite smoothening length in the RSOC profile and a magnetic field component h_z parallel to the spin-orbit field. For simplicity we focus on the optimal configuration $\alpha_L/\alpha_R = -1$ and $E_{\mathrm{SO},R} = 0.25$ meV, with a smoothening length $\lambda_s = 50$ nm. These are the parameters also used in Fig. 3(b), where we observe that, keeping a fixed value of the magnetic gap energy Δ_Z, and varying the additional parallel field component h_z represents a natural physical knob to control the weight and the existence of the bound state.

Figure 5 shows the spatial profile of the orthogonal spin density for $\Delta_Z = 0.50$ meV and for various values of h_z. In particular, Fig. 5(a) displays the full s_y, while Fig. 5(b) shows the bound state contribution $s_{y,\mathrm{bs}}$. Two features are noteworthy. In the first instance, as compared to the cuspid peaks obtained at the interface in the case of the sharp profile [Figs. 4(c) and 4(d)], the peaks of Fig. 5 are rounded off by the finite smoothening length λ_s. Second, while the peak of the full s_y [Fig. 5(a)] is very weakly affected by the parallel magnetic field component h_z, the bound state peak shown in Fig. 5(b) rapidly decreases and eventually disappears when the parallel magnetic field component h_z is ramped up, yielding a vanishing contribution (dashed line). This is in agreement with the binding energy behavior previously shown in Fig. 3(b), where one can see that, at $\Delta_Z = 0.50$ meV, the bound state disappears for $h_z = 0.50$ meV. The comparison between Figs. 5(a) and 5(b) clearly indicates that, when the bound state exists and has a relatively high binding energy, the peak of s_y is mainly due to it. However, when the binding energy decreases, the bound state contribution to the peak is replaced by the one of the excited states, so that the orthogonal spin density peak remains present.

V. DISCUSSION

We have demonstrated that the peak of the orthogonal spin density localized at the interface does not necessarily stem from a localized bound state, and appears to be a quite general feature. Two natural questions then arise, namely (i) what parameters characterizing the interface determine such peak? (ii) Can one explain its presence on some general principle? Here we wish to address these two questions.

A. General features of the orthogonal spin density

To answer the first question, we consider for definiteness the case of magnetic gap energy $\Delta_Z = 0.50$ meV and a maximal spin-orbit energy $E_{\mathrm{SO},R} = 0.25$ meV. Two parameters characterize the interface, namely the ratio α_L/α_R of the two RSOC, and the smoothening length of the profile. In Fig. 6(a) we show, for a fixed smoothening length $\lambda_s = 50$ nm, the orthogonal spin density profile for different values of the RSOC ratio α_L/α_R across the interface. As one can see, the height of the peak grows with the relative RSOC jump, in a roughly linear way.

In Fig. 6(b), keeping now the ratio of the two RSOC bulk values to $\alpha_L/\alpha_R = -1$, we vary the smoothening length λ_s of the profile. The peak decreases and broadens with increasing λ_s. Importantly, one can verify by a numerical integration that the area underneath each $s_y(x)$ profile is to a very good approximation *independent* of the value of the smoothening length λ_s.

B. Origin of the orthogonal spin density

Keeping in mind the two features described in the previous subsection, let us now discuss the origin of the orthogonal spin density peak. As is well know, a magnetic moment exposed to a magnetic field experiences a magnetic torque [64]. So is

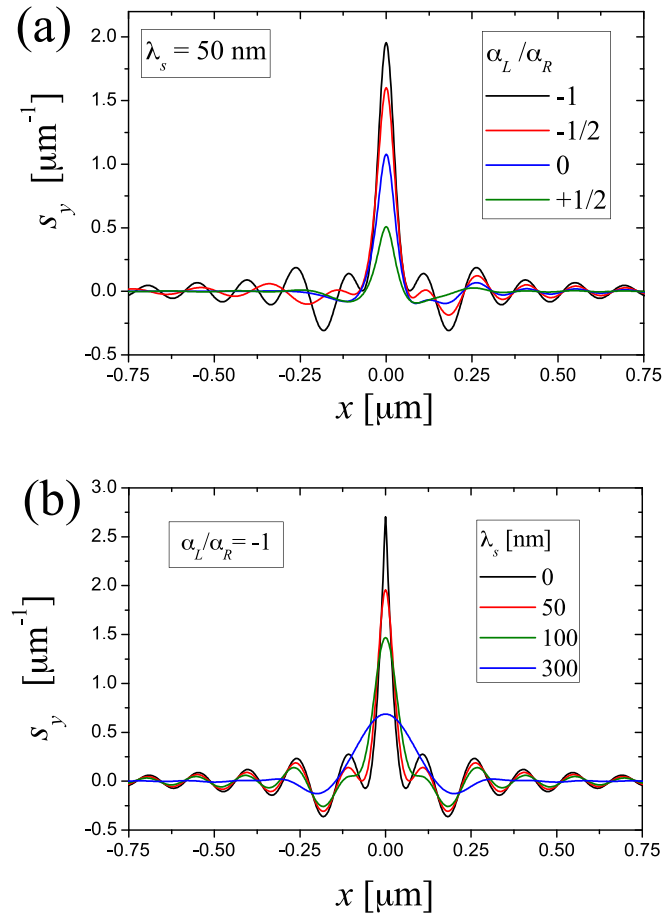

FIG. 6. Spatial profile of the orthogonal spin density for an interface with $E_{\mathrm{SO},R} = 0.25$ meV, and a magnetic gap energy $\Delta_Z = 0.50$ meV. (a) The effects of the ratio between the two values of RSOC, for a fixed smoothening length $\lambda_s = 50$ nm. (b) Effects of the smoothening length, for the configuration $\alpha_L/\alpha_R = -1$.

the case for spin magnetic moments of electrons moving in a NW, where both the externally applied magnetic field $\mathbf{h}$ and the effective spin-orbit field $\mathbf{h}^{\mathrm{SO}}$ give rise to corresponding torques, defined as

$$\hat{\mathbf{T}}^{h} \equiv \hat{\Psi}^{\dagger}(\boldsymbol{\sigma} \times \mathbf{h})\hat{\Psi}, \tag{20}$$

$$\hat{\mathbf{T}}^{\mathrm{SO}} \equiv \tfrac{1}{2}(\hat{\Psi}^{\dagger}(\boldsymbol{\sigma} \times \mathbf{h}^{\mathrm{SO}})\hat{\Psi} + \mathrm{H.c.}), \tag{21}$$

respectively, where

$$\mathbf{h}^{\mathrm{SO}}(x,t) = \frac{\{\alpha(x), p_x\}}{2\hbar}(0,0,1) \tag{22}$$

is the spin-orbit field. Note that, by definition Eqs. (21) and (22), the spin-orbit torque $\hat{\mathbf{T}}^{\mathrm{SO}} = (\hat{\mathrm{T}}^{\mathrm{SO}}_x, \hat{\mathrm{T}}^{\mathrm{SO}}_y, 0)$ has no component along the Rashba field direction z.

Importantly, the torques determine the spin dynamics through the operator identity

$$\partial_t \hat{\mathbf{S}} + \partial_x \hat{\mathbf{J}}^{s} = \hat{\mathbf{T}}^{h} + \hat{\mathbf{T}}^{\mathrm{SO}}, \tag{23}$$

where $\hat{\mathbf{S}}$ is the spin density operator in Eq. (17), and

$$\hat{\mathbf{J}}^s = \frac{\hbar}{2}\left(-\frac{i\hbar}{2m^*}[\hat{\Psi}^\dagger(x)\,\boldsymbol{\sigma}\,\partial_x\hat{\Psi}(x) - \partial_x\hat{\Psi}^\dagger(x)\,\boldsymbol{\sigma}\,\hat{\Psi}(x)] - \frac{\alpha(x)}{\hbar}\hat{\Psi}^\dagger(x)\,\frac{\{\boldsymbol{\sigma},\sigma_z\}}{2}\,\hat{\Psi}(x)\right) \tag{24}$$

is the spin current density operator [64,65]. Differently from the continuity equation for charge, in Eq. (23) the torques on the right-hand side play the role of sources and sinks of spin.

At equilibrium the expectation values of $\hat{\mathbf{S}}$ is time independent, while the one of the magnetic torque is straightforwardly related to the equilibrium spin-density Eq. (19), through $\mathbf{T}^h = \langle\hat{\mathbf{T}}^h\rangle_\circ = \mathbf{s}\times\mathbf{h}$. Thus, taking the equilibrium expectation value Eq. (23) one has

$$\partial_x\mathbf{J}^s = \mathbf{s}(x)\times\mathbf{h} + \mathbf{T}^{\mathrm{SO}}(x), \tag{25}$$

where $\mathbf{T}^{SO} = \langle\hat{\mathbf{T}}^{\mathrm{SO}}\rangle_\circ$. Let us focus on the most customary situation where the magnetic field is directed along the NW axis x ($\mathbf{h} = h_x\mathbf{i}_x$), i.e., orthogonal to the spin-orbit field. In this case, one can show that the spin-orbit torque $\mathbf{T}^{\mathrm{SO}}(x)$ vanishes, and that the spin current is oriented along z, so that Eq. (25) reduces to

$$\partial_x J^s_z = -h_x\, s_y(x). \tag{26}$$

We shall now argue that this equation, derived under quite general hypotheses, is the key to interpret the appearance of the orthogonal spin density at the interface, even when the bound state is absent.

Indeed, as has been demonstrated in Ref. [58], when uniform spin-orbit and magnetic fields are present in a NW, an equilibrium spin current J^s_z flows in its bulk. Such bulk spin current arises from the interplay between spin-orbit field and a magnetic field orthogonal to it, which induce nontrivial quantum correlation between spin and velocity, in close similarity to what happens in the helical states of a quantum spin Hall system. The bulk equilibrium spin current is odd in α and even in h_x. For example, for $\mu = 0$ and in the regime $\Delta_Z \gg E_{\mathrm{SO}}$, one has $J^s_z = -\mathrm{sgn}(\alpha)\sqrt{\Delta_Z E_{\mathrm{SO}}}/3\pi$. Equilibrium spin currents have been predicted for other RSOC systems as well [64–79] and, in fact, they can be regarded to as the diamagnetic color currents associated to the non-Abelian spin-orbit gauge fields [80]. However, its measurement in actual experiments has not been achieved thus far. In this respect, Eq. (26) suggests that, while the equilibrium spin current itself is perhaps elusive, its *variation* in the presence of inhomogeneities could be detected, as it is straightforwardly connected to the orthogonal spin density. Indeed, when two regions with different RSOC are connected, a kink $\partial_x J^s_z$ must arise at the interface to match the different spin current values in the two bulks. In view of Eq. (26), a peak in the orthogonal spin density s_y necessarily appears. This is the reason why the peak of s_y shown in Fig. 6(a) is more pronounced the higher the difference in the RSOC of the two regions. Furthermore, integrating both sides of Eq. (26), one can see that the integral of the s_y profile equals the difference between the two bulk spin currents, which is independent of the smoothening length. This is precisely what we found in Fig. 6(b). Finally, this argument is quite general and is not based on the existence of a bound state at the interface. This explains why the peak shown in Fig. 4(d) persists even when the bound state is absent, and shows that the naive interpretation of an orthogonal spin density localized peak in terms of a bound state is in general wrong.

C. The case of two interfaces

Thus far we have considered the case of one single interface along the NW. Here we wish to briefly discuss the case of two interfaces, modeling a NW inner region characterized by a RSOC parameter α_{in} sandwiched between two outer regions, where the RSOC shall be taken for simplicity equal to α_{out} in both. This corresponds to a profile

$$\alpha(x) = \alpha_{\mathrm{out}} + \frac{\alpha_{\mathrm{in}} - \alpha_{\mathrm{out}}}{2}\times\left\{\mathrm{Erf}\left[\frac{\sqrt{8}}{\lambda_s}\left(x+\frac{L}{2}\right)\right] - \mathrm{Erf}\left[\frac{\sqrt{8}}{\lambda_s}\left(x-\frac{L}{2}\right)\right]\right\}, \tag{27}$$

sketched in Fig. 7(a), where L denotes the length of the inner NW region, supposed to be much bigger than the smoothening length ($L \gg \lambda_s$), so that the notion of interfaces still makes sense. When the distance L is much larger than the typical variation length scale for observables in the single interface problem, the two interfaces act independently. However, when such two scales become comparable, noteworthy aspects emerge, which are illustrated in Fig. 7.

First, if the interface bound states exist, they overlap across the distance L, causing a splitting of their degeneracy. The density profile of the resulting lowest eigenstate is mainly peaked at the interfaces, but is nonvanishing also in the center of the inner region, as illustrated by the black curve in Fig. 7(b). Second, even if the interface bound states are not present, another type of bound states may appear. Indeed, when the inner region is Rashba dominated and $|\alpha_{\mathrm{in}}| > |\alpha_{\mathrm{out}}|$, the band bottom of the inner region is lower than in the outer regions. Thus, for short L the two interfaces give rise to an effective Rashba quantum dot [59,60], with discrete bound states localized within the confinement length L. This is the case depicted by the red curve in Fig. 7(b), where the density profile of the lowest eigenstate corresponds to a Rashba dot bound state. Such quantum dot bound states thus have a completely different origin from the interface bound states. In particular, while the interface bound states are present only in the presence of an applied magnetic field, the Rashba dot bound states are intrinsic, as they may also be present without magnetic field [81].

The third interesting feature of the double interface problem is that, in all cases, pronounced orthogonal spin density peaks appear at the interfaces, regardless of whether interface bound states exist or not. Remarkably, the signs of the peaks are *opposite* at the two interfaces, as shown in Fig. 7(c). This is because the opposite jump in the RSOC across the two interfaces causes two opposite kinks in the equilibrium spin current, as observed in Sec. V B. Thus, despite the NW is in the topologically trivial phase, the emerging scenario is identical to the one occurring in a NW in the topological phase, where the spin density of the MQPs is orthogonal to both the magnetic field and the RSOC field direction,

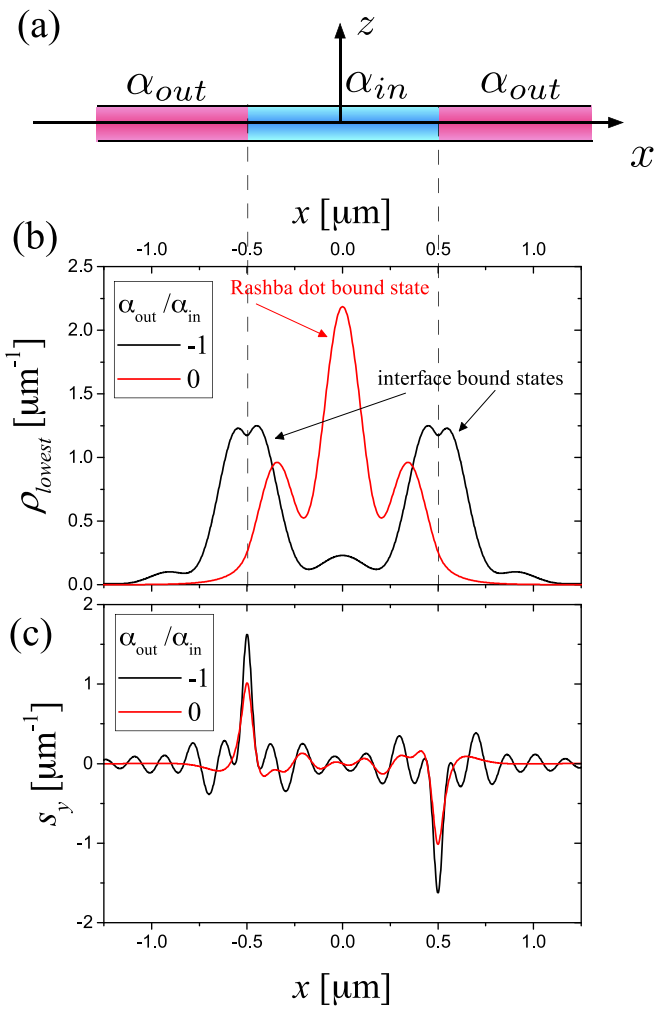

FIG. 7. (a) Sketch of a double interface problem, modeled by the RSOC profile (27). The parameters are $L = 1$ μm, $\lambda_s = 50$ nm, the value $\alpha_{in} > 0$ in the inner region corresponds to $E_{SO,in} = 0.25$ meV, while the magnetic gap energy is $\Delta_Z = 0.25$ meV. (b) The density profile of the lowest electron state, for two values $\alpha_{out} = -\alpha_{in}$ (black curve) and $\alpha_{out} = 0$ (red curve), showing the difference between interface and Rashba dot bound states. (c) The total orthogonal spin density, for the same two values of α_{in}, shows two opposite peaks at the interfaces.

and takes opposite signs at the two NW ends [47–49]. This explicitly demonstrates that such orthogonal spin polarization pinned at the NW ends can neither be taken as a hallmark of the topological phase nor as an evidence of bound states. Note also that the orthogonal spin polarization peaks are typically narrower than the interface bound state and are thus more robust to finite length L effects too.

D. Possible setup realizations

Several experiments in topological systems are based on InSb [30,34,52,82–84] or InAs [33,50,53,85–87] NWs deposited on a substrate. In the case of InSb the effective mass and the g factor are $m^* \simeq 0.015\ m_e$ and $g \simeq 50$, respectively, while the value of the RSOC depends on the specific implementation and experimental conditions and can be widely tunable, ranging from $\alpha \sim 0.03$ eV Å to $\alpha \sim 1$ eV Å [27,30,50,52,82,83]. The spin-orbit energy E_{SO} resulting from these values [see Eq. (5)] is a fraction of meV. The same order of magnitude is obtained for the magnetic gap energy Δ_Z in a magnetic field range of some hundreds of mT. These are the values adopted in our plots. Similarly, in the case of InAs nanowires $m^* \simeq 0.022\ m_e$, $g \simeq 20$ and the RSOC ranges from $\alpha \sim 0.05$ to $\alpha \sim 0.3$ eV Å [29,50,85,86]. The temperature value of 250 mK used in our plots is state of the art with modern refrigeration techniques.

Interfaces between regions with different RSOC emerge quite naturally in typical NW setups, where a portion of the NW is covered by, e.g., a superconductor or by a normal metal to induce proximity effect, to measure the current, or to locally vary the potential. The resulting SIA is inhomogeneous along the NW, and can be controlled, e.g., by the application of different gate voltage values applied to top/bottom gates or to the substrate, similarly to the case of constrictions in quantum spin Hall systems [88–90]. In particular, covering one portion with the gate-all-around technique and by applying a sufficiently strong gate voltage, it is reasonable to achieve an inversion of the sign of the RSOC as compared to the uncovered NW portion, as has already been done in similar setups [51,57,91–93].

Finally, the orthogonal spin polarization predicted here can be measured by spatially resolved detection of spin orientation. In particular, nanometer scale resolution can be reached with various methods such as magnetic resonance force microscopy [94,95], spin-polarized scanning electron microscopy [96,97], by using quantum dots as probes [98,99], or also electrically by potentiometric measurements exploiting ferromagnetic detector contacts [100,101].

VI. CONCLUSIONS

In conclusion, in this paper we have considered a NW with an interface between two regions with different RSOC values, as sketched in Fig. 1, when proximity effect is turned off and the NW is in the topologically trivial phase.

In Sec. III we have shown that at the interface bound states may appear, whose energy is located below the continuum spectrum minimum. Such bound states are neither topological (since proximity effect is absent) nor intrinsic interface bound states (since they only exist if an external magnetic field is applied along the NW axis). Analyzing first the case of a sharp interface RSOC profile Eq. (13), we have obtained the phase diagram determining the existence of the bound state [see Fig. 2(a)], as well as the dependence of its binding energy on the magnetic gap energy [see Fig. 2(b)]. While the bound state always exists if the RSOC takes equal and opposite values across the interface (optimal configuration), for all other situations it only exists if the magnetic field overcomes a minimal threshold value. Furthermore, even in the optimal configuration, it can be suppressed by either a finite smoothening length in the RSOC profile or a magnetic field component parallel to the spin-orbit field (see Fig. 3).

In Sec. IV we have then investigated the spatial profile of the charge density ρ and the spin density, with a special focus on the spin density component s_y, orthogonal to both the applied magnetic field and the RSOC field direction, which is known to characterize the MQPs localized at the edges

of a NW in the topological phase. By analyzing both the full equilibrium values ρ and s_y due to all occupied states, and the bound state contributions $\rho_{\rm bs}$ and $s_{y,\rm bs}$, we have been able to gain two useful insights. First, the orthogonal spin density appears also in the topologically trivial phase as a quite general effect characterizing any interface between two different RSOC regions under a magnetic field. This extends our previous results of Ref. [58] related to NW contacted to normal leads without RSOC. Second, for realistic and typical values of chemical potential and temperature, the orthogonal spin density peak is relatively robust to parameter changes, and persists even when the bound state is absent (see Figs. 4 and 5). This means that also the propagating states of the continuum spectrum modify their spin texture around the interface to preserve the peak, so that a localized orthogonal spin density cannot be considered a signature of a bound state.

Furthermore, in Sec.V, after analyzing in Fig. 6 the peak dependence on the single interface parameters, we have addressed the case of two interfaces (see Fig. 7). While for a large distance L between the interfaces the single-interface scenario is merely doubled, for a shorter L the interface bound states may overlap and additional Rashba quantum dot states may appear. In all cases, and independently of the presence of interface bound states, the spin density s_y, *orthogonal* to both the magnetic field and the Rashba spin-orbit field, exhibits relatively robust peaks taking *opposite signs* at the two interfaces [see Fig. 7(c)]. Remarkably, these are the same features predicted for the spin density of the MQPs emerging at the ends of a NW in the topological phase, despite the NW considered here is in the topologically trivial phase. Our results thus show that such orthogonal spin polarization pinned at the NW ends can neither be taken as a hallmark of the topological phase nor as an evidence of bound states.

However, we have also shown in Sec. V that such stable peaks may in fact have an impact on the detection of spin currents. Indeed a spin current flows in the bulk of a NW as a result of quantum correlations between spin and velocity induced by the interplay between magnetic and spin-orbit field, similarly to the case of quantum spin Hall helical states. Despite various proposals in the literature, the measurement of equilibrium spin currents has not been achieved yet. Our results suggest that, while the equilibrium spin current itself may be elusive, its variations can be detected through the orthogonal spin density s_y, which is instead experimentally observable with spin-resolved detection techniques. Indeed the orthogonal spin density peak is precisely related to the kink of the spin current localized at the interface. With the provided description of possible implementations in realistic NW setups, the predicted effects seem to be at experimental reach.

ACKNOWLEDGMENTS

Fruitful discussions with M. Sassetti, F. Cavaliere, and N. Traverso Ziani are greatly acknowledged. Computational resources were provided by hpc@polito at Politecnico di Torino.

APPENDIX A: CALCULATION FOR SHARP PROFILE INTERFACE

In this Appendix we provide details about the calculation for a sharp profile interface (13). In such a situation the eigenvalue equation stemming from the Hamiltonian (2) at energy E reads

$$\begin{pmatrix} -\frac{\hbar^2}{2m^*}\partial_x^2 + i\alpha(x)\partial_x + i\frac{\alpha_R-\alpha_L}{2}\delta(x) - h_z & -h_x \\ -h_x & -\frac{\hbar^2}{2m^*}\partial_x^2 - i\alpha(x)\partial_x - i\frac{\alpha_R-\alpha_L}{2}\delta(x) + h_z \end{pmatrix} \begin{pmatrix} \psi_\uparrow^{(E)}(x) \\ \psi_\downarrow^{(E)}(x) \end{pmatrix} = E \begin{pmatrix} \psi_\uparrow^{(E)}(x) \\ \psi_\downarrow^{(E)}(x) \end{pmatrix} \tag{A1}$$

equipped with the boundary conditions at the interface

$$\begin{cases} \psi_\uparrow(0^-) = \psi_\uparrow(0^+), \\ \psi_\downarrow(0^-) = \psi_\downarrow(0^+), \\ \partial_x\psi_\uparrow(0^-) = \partial_x\psi_\uparrow(0^+) - i\frac{m^*}{\hbar^2}(\alpha_R - \alpha_L)\psi_\uparrow(0), \\ \partial_x\psi_\downarrow(0^-) = \partial_x\psi_\downarrow(0^+) + i\frac{m^*}{\hbar^2}(\alpha_R - \alpha_L)\psi_\downarrow(0). \end{cases} \tag{A2}$$

A few remarks about the boundary conditions (A2) are in order. First, the discontinuity in the derivative of the wave function involves an imaginary unit too, making such boundary conditions intrinsically different from the ones of the well known problem of a particle in a scalar δ potential. Second, as a consequence of such imaginary unit, it can straightforwardly be shown that, despite the derivative $\partial_x\psi_s$ is discontinuous ($s = \uparrow, \downarrow$), the derivative $\partial_x\rho_s$ of the quantity $\rho_s(x) \equiv \psi_s^*(x)\psi_s(x)$ is *continuous* at the interface $x = 0$. For this reason, both the density $\rho(x) = \rho_\uparrow + \rho_\downarrow$ [see Eq. (18)] and the spin density component $s_z = \rho_\uparrow - \rho_\downarrow$ [see Eq. (19)] do not exhibit any cusp in their spatial profile. In contrast, off-diagonal spin density components s_x and s_y, which cannot be expressed in terms of the ρ_s's, do exhibit a cusp due to the discontinuity of the derivative implied by the boundary conditions (A2). This difference becomes apparent by comparing, e.g., Figs. 4(b) and 4(d).

Let us now proceed with the calculation of the energy spectrum. As observed above, we have assumed $\alpha_R > 0$ and $|\alpha_L| \leqslant |\alpha_R|$ without loss of generality. As a consequence $E_{{\rm SO},R}$ is the higher spin-orbit energy, $E_{{\rm SO},R} \geqslant E_{{\rm SO},L}$ [see Eq. (10)]. By denoting the ratio between the two RSOC values

$$r \equiv \frac{\alpha_L}{\alpha_R} \quad \in [-1\,,\,1] \tag{A3}$$

one has $E_{{\rm SO},L} = r^2 E_{{\rm SO},R}$. One can introduce the momentum space Hamiltonian $H_k^\nu = \varepsilon_k^0 - \alpha_\nu k\sigma_z - h_x\sigma_x - h_z\sigma_z$ describing the homogeneous bulk of each side $\nu = R/L$ of the interface, and match the related eigenfunctions with the boundary conditions (A2).

The energy spectrum characterizing the NW on the right-hand side and on the left-hand side of the interface can be suitably rewritten as

$$E_\pm^R(K) = \frac{K^2}{4E_{{\rm SO},R}} \pm \sqrt{\Delta_Z^2 + (K + h_z)^2}, \tag{A4}$$

$$E^L_{\pm}(K) = \frac{(rK)^2}{4E_{\mathrm{SO},L}} \pm \sqrt{\Delta_Z^2 + (rK + h_z)^2}, \tag{A5}$$

respectively, where $K = \alpha_R k$ has the dimension of an energy, while Δ_Z is the magnetic gap energy Eq. (4).

The eigenstates of the momentum Hamiltonian in each side can be written, for arbitrary complex wave vector K, in the following explicit form:

$$\text{for } x > 0 \quad \begin{cases} w_-(K) &= \frac{1}{\sqrt{\Delta_Z^2 + |z(K)|^2}} \begin{pmatrix} z(K) \\ \Delta_Z \end{pmatrix}, \\ w_+(K) &= \frac{1}{\sqrt{\Delta_Z^2 + |z(K)|^2}} \begin{pmatrix} -\Delta_Z \\ z(K) \end{pmatrix}, \end{cases} \tag{A6}$$

$$\text{for } x < 0 \quad \begin{cases} w_-(rK) &= \frac{1}{\sqrt{\Delta_Z^2 + |z(rK)|^2}} \begin{pmatrix} z(rK) \\ \Delta_Z \end{pmatrix}, \\ w_+(rK) &= \frac{1}{\sqrt{\Delta_Z^2 + |z(rK)|^2}} \begin{pmatrix} -\Delta_Z \\ z(rK) \end{pmatrix}, \end{cases} \tag{A7}$$

where $z(K) = \sqrt{\Delta_Z^2 + (K + h_z)^2} + (K + h_z)$.

In order to determine the energy E_{bs} of the bound state, the crucial point is to correctly re-express Eqs. (A6) and (A7) as a function of the energy E, and then to impose the boundary conditions (A2). To this purpose, the first step is to invert the dispersion relation in each side $\nu = R/L$. This can be done analytically in two specific cases, namely for $h_z = 0$ or for $h_x = 0$. Here below we shall discuss these two situations, while the general case $h_x, h_z \neq 0$ will be approached numerically as described in Appendix B.

1. The case $h_z = 0$

In this case the dispersion relation can be inverted yielding four possible K values

$$K^{\nu}_{\epsilon,\epsilon'}(E) = \epsilon \sqrt{4E_{\mathrm{SO},R}\left[E + 2E_{\mathrm{SO},\nu} + \epsilon' \sqrt{\Delta_Z^2 + 4E^2_{\mathrm{SO},\nu} + 4E_{\mathrm{SO},\nu}E}\right]}, \tag{A8}$$

where $\epsilon, \epsilon' = \pm 1$. Note that $K \in \mathbb{C}$, and we have adopted the convention $\sqrt{z} = \sqrt{|z|}e^{i\frac{\phi}{2}}$ for the square root of a complex number $z = |z|e^{i\phi}$ with $\phi \in (-\pi\ ,\ \pi\ ]$.

One then inserts the four possible values (A8) of $K^{\nu}_{\epsilon,\epsilon'}$ into the two eigenvectors Eqs. (A6) and (A7). In doing that, some caution must be taken, since for a given energy E and each side of the interface a seeming redundancy of eigenstates appears. However, only half of the possible eigenstates actually fulfill the equation $H_k[K(E)]w[K(E)] = E\, w[K(E)]$, as it should be. Their explicit expressions depend on the regime of the involved energy scales E, Δ_Z, and $E_{\mathrm{SO},\nu}$, Focusing, e.g., on the right-hand side of the interface, one can identify three regimes where, for a given energy E lower than the overall minimum of the bulk bands, the corresponding four correct eigenspinors are given in Eq. (A9).

Regime 2 differs from regime 3 because in the former wave vectors turn out to be strictly imaginary, while in the latter they exhibit a real part as well. The expression for the eigenspinors on the left-hand side, together with their corresponding domain, can be directly obtained from the ones in (A9) by simply replacing $E_{\mathrm{SO},R} \to E_{\mathrm{SO},L}$ and $K^R_{\pm\pm}(E) \to r\, K^L_{\pm\pm}(E)$.

Regime	Eigenvectors
1) $\Delta_Z > 4E_{\mathrm{SO},R}$ and $-\dfrac{\Delta_Z^2 + 4E^2_{\mathrm{SO},R}}{4E_{\mathrm{SO},R}} < E < -\Delta_Z$	$w_-\left[K^R_{\epsilon,+}(E)\right]$, $w_+\left[K^R_{\epsilon,+}(E)\right]$ $\quad \epsilon = \pm 1$
2) $\Delta_Z > 2E_{\mathrm{SO},R}$ and $-\dfrac{\Delta_Z^2 + 4E^2_{\mathrm{SO},R}}{4E_{\mathrm{SO},R}} < E < \min\left[-\dfrac{\Delta_Z^2}{4E_{\mathrm{SO},R}}, -\Delta_Z\right]$	$w_-\left[K^R_{\epsilon,\epsilon'}(E)\right]$ $\quad \epsilon, \epsilon' = \pm 1$
3) $\Delta_Z < 4E_{SO,R}$ and $E < -\dfrac{\Delta_Z^2 + 4E^2_{\mathrm{SO},R}}{4E_{\mathrm{SO},R}}$	$w_-\left[K^R_{\epsilon,\epsilon'}(E)\right]$ $\quad \epsilon, \epsilon' = \pm 1$

(A9)

Once the four eigenspinors w and momenta K are identified, the wave function ψ is constructed as a linear superposition of each spinor w multiplied by the related phase factor e^{iKx/α_R}. In doing that, the requirement that ψ does not diverge at $x \to \pm\infty$ reduces the four terms to two in each side. Let thus $w^{\nu}_j(E)$ and $K^{\nu}_j(E)$ with $j = 1, 2$ denote such two eigenspinors and momenta related to nondivergent wave functions in the region $\nu = R/L$ at energy E in a given regime. Then the eigenfunction $\psi^{(E)}(x)$ can be written as a linear superposition

$$\psi^{(E)}(x) = \begin{cases} \sum_{j=1}^2 l_j w^R_j(E)\, e^{i\frac{K^R_j(E)}{\alpha_R}x}, & x > 0, \\ \sum_{j=1}^2 r_j w^L_j(E)\, e^{i\frac{K^L_j(E)}{\alpha_R}x}, & x < 0. \end{cases} \tag{A10}$$

Thus, the boundary condition Eq. (A2) leads to a homogeneous system of four linear equations in four unknowns l_1, l_2, r_1, and r_2. Imposing the solvability of the system one obtains an equation for the energy E whose solutions, if they exist, correspond to the energy E_b of the bound state for given values of Δ_Z, $E_{\mathrm{SO},R}$, and r. The binding energy (12) is then straightforwardly obtained.

2. The case $h_x = 0$

In this case the eigenvalue problem (A1) decouples into two separate problems for the spin-↑ and spin-↓ components of the wave function, and the magnetic gap energy $\Delta_Z = |h_x|$ vanishes. Accordingly, the eigenvectors (A6) acquire the simple form

$$w_-(K)|_{\Delta_Z=0} = \begin{pmatrix} 1 \\ 0 \end{pmatrix}, \quad w_+(K)|_{\Delta_Z=0} = \begin{pmatrix} 0 \\ 1 \end{pmatrix} \tag{A11}$$

both for $x > 0$ and $x < 0$, while the eigenvalues have a quadratic dependence on K,

$$\begin{cases} E^R_\uparrow(K) = \frac{K^2}{4E_{SO,R}} - (K + h_z), & x > 0, \\ E^L_\uparrow(K) = \frac{(rK)^2}{4E_{SO,L}} - (rK + h_z), & x < 0, \\ E^R_\downarrow(K) = \frac{K^2}{4E_{SO,R}} + (K + h_z), & x > 0, \\ E^L_\downarrow(K) = \frac{(rK)^2}{4E_{SO,L}} + (rK + h_z), & x < 0. \end{cases} \tag{A12}$$

Without loss of generality, we can focus on the spin-↑ component of the wave function. The dispersion relation can be easily inverted

$$\begin{cases} K^R_\pm(E) = 2E_{\mathrm{SO},R} \pm \sqrt{(2E_{\mathrm{SO},R})^2 + 4E_{\mathrm{SO},R}(h_z + E)}, \\ K^L_\pm(E) = 2rE_{\mathrm{SO},R} \pm \sqrt{(2rE_{\mathrm{SO},R})^2 + 4E_{\mathrm{SO},R}(h_z + E)}. \end{cases} \tag{A13}$$

In order for $K^\nu_\pm(E)$ to exhibit an imaginary part, one has to consider energies in the range $E < -h_z - E_{\mathrm{SO},\nu}$ and the most general eigenfunction of energy E can thus be written as

$$\psi^{(E)}(x) = \begin{cases} a\, e^{i\frac{K^R_+(E)}{\alpha_R}x} + b\, e^{i\frac{K^R_-(E)}{\alpha_R}x}, & x > 0, \\ c\, e^{i\frac{K^L_+(E)}{\alpha_R}x} + d\, e^{i\frac{K^L_-(E)}{\alpha_R}x}, & x < 0, \end{cases} \tag{A14}$$

where a, b, c, d are complex coefficients to be determined. The regularity at $x \to \pm\infty$ and the continuity in $x = 0$ reduce the wave function to the form

$$\psi^{(E)}(x) = \begin{cases} a\, e^{\frac{iK^R_+(E)x}{\alpha_R}}, & x > 0, \\ a\, e^{\frac{iK^L_-(E)x}{\alpha_R}}, & x < 0, \end{cases} \tag{A15}$$

while the matching condition (A2) on the first derivative in $x = 0$ implies

$$K^L_-(E) = K^R_+(E) - 2E_{\mathrm{SO},R}(1 - r) \tag{A16}$$

whose only possible solution is

$$\begin{cases} r^2 = 1, \\ E = -h_z - E_{\mathrm{SO},R}. \end{cases} \tag{A17}$$

However, this corresponds to the lowest energy eigenfunction of the continuum, demonstrating that no bound state exists in such case.

APPENDIX B: DIAGONALIZATION STRATEGY IN THE PRESENCE OF A SMOOTHENING LENGTH

Here we describe how to numerically approach the problem in the presence of the RSOC profile (15) characterized by a finite smoothening length λ_s, and when both perpendicular and parallel magnetic field components $h_x, h_z \neq 0$ are present. To this end, we impose periodic boundary conditions onto the NW, and express the electron spinor field in terms of discretized Fourier components $k = 2\pi n/\Omega$, namely

$$\hat\Psi(x) = \sum_k \frac{e^{ikx}}{\sqrt{\Omega}} \begin{pmatrix} \hat c_{k\uparrow} \\ \hat c_{k\downarrow} \end{pmatrix}, \tag{B1}$$

where Ω is the (large) NW periodicity length and $\hat c_{k,s}$ denotes the Fourier mode operators for spin $s = \uparrow, \downarrow$. The Hamiltonian (1) is thus rewritten in terms of the discretized k basis introduced in Eq. (B1) as

$$\hat{\mathcal{H}} = \sum_{k_1,k_2} \sum_{s_1,s_2=\uparrow,\downarrow} \hat c^\dagger_{k_1,s_1} H_{k_1,s_1;k_2s_2}\, \hat c_{k_2,s_2}, \tag{B2}$$

where

$$H_{k_1,s_1;k_2s_2} = \Big[\big(\varepsilon^0_{k_1}\sigma_0 - \mathbf{h}\cdot\boldsymbol{\sigma}\big)\delta_{k_1,k_2} - \alpha_{k_1-k_2}\frac{k_1+k_2}{2}\,\sigma_z \Big]_{s_1,s_2}, \tag{B3}$$

where α_q is the (discretized) Fourier transform of the RSOC profile $\alpha(x)$. Specifically, taking for α_q the following expression:

$$\alpha_q = \begin{cases} \frac{\alpha_L+\alpha_R}{2}, & \text{for } q = 0, \\ e^{-\frac{q^2\lambda_s^2}{32}}\, \frac{\alpha_L(e^{\frac{iq\Omega}{2}}-1) - \alpha_R(e^{-\frac{iq\Omega}{2}}-1)}{iq\Omega}, & \text{otherwise}, \end{cases} \tag{B4}$$

one obtains the (periodic version) of the prototypical profile Eq. (15) as Fourier series $\alpha(x) = \sum_q \alpha_q e^{iqx}$.

Then we have performed an exact numerical diagonalization of the Hamiltonian matrix Eq. (B3), thereby obtaining diagonalizing operators $\hat d_\xi$ defined through $\hat c_a = \sum_\xi U_{a,\xi}\,\hat d_\xi$, where $a = (k, s)$ is a compact quantum number notation for the original basis, and U is the matrix of the eigenvectors of Eq. (B3). Denoting by E_ξ the eigenvalues, the NW Hamiltonian can be rewritten as

$$\hat{\mathcal{H}} = \sum_\xi E_\xi\, \hat d^\dagger_\xi \hat d_\xi. \tag{B5}$$

Finally, to compute the equilibrium expectation values $\langle\cdots\rangle_\circ$ of the operators (16) and (17), one can reexpress the electron field operator $\Psi_s(x)$ with spin component $s = \uparrow, \downarrow$ in terms of the diagonalizing operators $\hat d_\xi$'s,

$$\hat\Psi_s(x) = \frac{1}{\sqrt{\Omega}} \sum_{k,\xi} e^{ikx} U_{ks,\xi}\, \hat d_\xi \tag{B6}$$

and to exploit $\langle \hat d^\dagger_\xi \hat d_{\xi'}\rangle_\circ = \delta_{\xi\xi'} f^\circ(E_\xi)$, with $f^\circ(E) = \{1 + \exp[(E-\mu)/k_BT]\}^{-1}$ denoting the Fermi distribution function. For instance, the density Eq. (18) is obtained as $\rho(x) = \sum_\xi \rho_\xi(x)$, where

$$\rho_\xi(x) = \frac{1}{\Omega} \sum_{s=\uparrow,\downarrow} \sum_{k_1,k_2} e^{-i(k_1-k_2)x}\, U^*_{k_1s,\xi} U_{k_2s,\xi}\, f^\circ(E_\xi) \tag{B7}$$

is the contribution arising from the ξth eigenstate. In this way, the contribution of each eigenstate (in particular the bound state) can be singled out.

[1] M. Z. Hasan and C. L. Kane, Rev. Mod. Phys. **82**, 3045 (2010).
[2] X.-L. Qi and S.-C. Zhang, Rev. Mod. Phys. **83**, 1057 (2011).
[3] M. Sato and Y. Ando, Rep. Prog. Phys. **80**, 076501 (2017).
[4] W. P. Su, J. R. Schrieffer, and A. J. Heeger, Phys. Rev. Lett. **42**, 1698 (1979).
[5] W. P. Su, J. R. Schrieffer, and A. J. Heeger, Phys. Rev. B **22**, 2099 (1980).
[6] C. L. Kane and T. C. Lubensky, Nat. Phys. **10**, 39 (2014).
[7] C. L. Kane and E. J. Mele, Phys. Rev. Lett. **95**, 146802 (2005).
[8] C. L. Kane and E. J. Mele, Phys. Rev. Lett. **95**, 226801 (2005).
[9] B. A. Bernevig, T. L. Hughes, and S.-C. Zhang, Science **314**, 1757 (2006).
[10] C. Liu, T. L. Hughes, X.-L. Qi, K. Wang, and S.-C. Zhang, Phys. Rev. Lett. **100**, 236601 (2008).
[11] M. König, H. Buhmann, L. W. Molenkamp, T. Hughes, C.-X. Liu, X.-L. Qi, and S.-C. Zhang, J. Phys. Soc. Jpn. **77**, 031007 (2008).
[12] A. Y. Kitaev, Phys. Usp. **44**, 131 (2001).
[13] J. Alicea, Rep. Progr. Phys. **75**, 076501 (2012).
[14] M. Sato and S. Fujimoto, J. Phys. Soc. Jpn. **85**, 072001 (2016).
[15] R. Aguado, Rivista del Nuovo Cimento **40**, 523 (2017).
[16] Y. Oreg, G. Refael, and F. von Oppen, Phys. Rev. Lett. **105**, 177002 (2010).
[17] R. M. Lutchyn, J. D. Sau, and S. Das Sarma, Phys. Rev. Lett. **105**, 077001 (2010).
[18] S. Nadj-Perge, I. K. Drozdov, B. A. Bernevig, and A. Yazdani, Phys. Rev. B **88**, 020407(R) (2013).
[19] L. Fu and C. L. Kane, Phys. Rev. Lett. **100**, 096407 (2008).
[20] J. Nilsson, A. R. Akhmerov, and C. W. J. Beenakker, Phys. Rev. Lett. **101**, 120403 (2008).
[21] F. Crépin, B. Trauzettel, and F. Dolcini, Phys. Rev. B **89**, 205115 (2014).
[22] C. Nayak, S. H. Simon, A. Stern, M. Freedman, and S. Das Sarma, Rev. Mod. Phys. **80**, 1083 (2008).
[23] D. Aasen, M. Hell, R. V. Mishmash, A. Higginbotham, J. Danon, M. Leijnse, T. S. Jespersen, J. A. Folk, C. M. Marcus, K. Flensberg, and J. Alicea, Phys. Rev. X **6**, 031016 (2016).
[24] T. D. Stanescu and S. Das Sarma, Phys. Rev. B **97**, 045410 (2018).
[25] T. E. O'Brien, P. Rożek, and A. R. Akhmerov, Phys. Rev. Lett. **120**, 220504 (2018).
[26] H. Zhang, D. E. Liu, M. Wimmer, and L. P. Kouwenhoven, Nat. Commun. **10**, 5128 (2019).
[27] V. Mourik, K. Zuo, S. M. Frolov, S. R. Plissard, E. P. A. M. Bakkers, and L. P. Kouwenhoven, Science **336**, 1003 (2012).
[28] L. P. Rokhinson, X. Liu, and J. K. Furdyna, Nat. Phys. **8**, 795 (2012).
[29] A. Das, Y. Ronen, Y. Most, Y. Oreg, M. Heiblum, and H. Shtrikman, Nat. Phys. **8**, 887 (2012).
[30] M. T. Deng, C. L. Yu, G. Y. Huang, M. Larsson, P. Caroff, and H. Q. Xu, Nano Lett. **12**, 6414 (2012).
[31] E. J. H. Lee, X. Jiang, M. Houzet, R. Aguado, C. M. Lieber, and S. De Franceschi, Nat. Nanotechnol. **9**, 79 (2014).
[32] S. M. Albrecht, A. P. Higginbotham, M. Madsen, F. Kuemmeth, T. S. Jespersen, J. Nygård, P. Krogstrup, and C. M. Marcus, Nature (London) **531**, 206 (2016).
[33] M. T. Deng, S. Vaitiekenas, E. B. Hansen, J. Danon, M. Leijnse, K. Flensberg, J. Nygård, P. Krogstrup, and C. M. Marcus, Science **354**, 1557 (2016).
[34] Ö. Gül, H. Zhang, J. D. S. Bommer, M. W. A. de Moor, D. Car, S. R. Plissard, E. P. A. M. Bakkers, A. Geresdi, K. Watanabe, T. Taniguchi, and L. P. Kouwenhoven, Nat. Nanotechnol. **13**, 192 (2018).
[35] E. J. H. Lee, X. Jiang, R. Aguado, G. Katsaros, C. M. Lieber, and S. De Franceschi, Phys. Rev. Lett. **109**, 186802 (2012).
[36] J. Liu, A. C. Potter, K. T. Law, and P. A. Lee, Phys. Rev. Lett. **109**, 267002 (2012).
[37] H. Pan and S. Das Sarma, Phys. Rev. Res. **2**, 013377 (2020).
[38] C.-X. Liu, J. D. Sau, T. D. Stanescu, and S. Das Sarma, Phys. Rev B **96**, 075161 (2017).
[39] J. Klinovaja and D. Loss, Eur. Phys. J. B **88**, 62 (2015).
[40] C. Fleckenstein, F. Domínguez, N. Traverso Ziani, and B. Trauzettel, Phys. Rev B **97**, 155425 (2018).
[41] J. Chen, B. D. Woods, P. Yu, M. Hocevar, D. Car, S. R. Plissard, E. P. A. M. Bakkers, T. D. Stanescu, and S. M. Frolov, Phys. Rev Lett. **123**, 107703 (2019).
[42] L. S. Ricco, M. de Souza, M. S. Figueira, I. A. Shelykh, and A. C. Seridonio, Phys. Rev B **99**, 155159 (2019).
[43] T. D. Stanescu and S. Tewari, Phys. Rev. B **100**, 155429 (2019).
[44] E. Prada, P. San-José, M. W. A. de Moor, A. Geresdi, E. J. H. Lee, J. Klinovaja, D. Loss, J. Nygård, R. Aguado, and L. P. Kouwenhoven, arXiv:1911.04512.
[45] F. Ronetti, K. Plekhanov, D. Loss, and J. Klinovaja, arXiv:1911.03133.
[46] S. Nadj-Perge, I. K. Drozdov, J. Li, H. Chen, S. Jeon, J. Seo, A. H. MacDonald, B. A. Bernevig, and A. Yazdani, Science **347**, 602 (2014).
[47] D. Sticlet, C. Bena, and P. Simon, Phys. Rev. Lett. **108**, 096802 (2012).
[48] K. Björnson, S. S. Pershoguba, A. V. Balatsky, and A. M. Black-Schaffer, Phys. Rev. B **92**, 214501 (2015).
[49] M. M. Maśka and T. Domański, Sci. Rep. **7**, 16193 (2017).
[50] D. Liang and X. P. A. Gao, Nano Lett. **12**, 3263 (2012).
[51] B. Slomski, G. Landolt, S. Muff, F. Meier, J. Osterwalder, and J. H. Dil, New J. Phys. **15**, 125031 (2013).
[52] I. van Weperen, B. Tarasinski, D. Eeltink, V. S. Pribiag, S. R. Plissard, E. P. A. M. Bakkers, L. P. Kouwenhoven, and M. Wimmer, Phys. Rev. B **91**, 201413(R) (2015).
[53] Z. Scherübl, G. Fülöp, M. H. Madsen, J. Nygård, and S. Csonka, Phys. Rev. B **94**, 035444 (2016).
[54] K. Takase, Y. Ashikawa, G. Zhang, K. Tateno, and S. Sasaki, Sci. Rep. **7**, 930 (2017).
[55] J. Borge and I. V. Tokatly, Phys. Rev. B **96**, 115445 (2017).
[56] Ch. Kloeffel, M. J. Rančić, and D. Loss, Phys. Rev. B **97**, 235422 (2018).
[57] H. Tsai, S. Karube, K. Kondou, N. Yamaguchi, and Y. Otani, Sci. Rep. **8**, 5564 (2018).
[58] F. Dolcini and F. Rossi, Phys. Rev. B **98**, 045436 (2018).
[59] D. Sánchez and L. Serra, Phys. Rev. B **74**, 153313 (2006).
[60] D. Sánchez, L. Serra, and M.-S. Choi, Phys. Rev. B **77**, 035315 (2008).
[61] M. Cheng and R. M. Lutchyn, Phys. Rev. B **86**, 134522 (2012).
[62] P. Szumniak, D. Chevallier, D. Loss, and J. Klinovaja, Phys. Rev. B **96**, 041401(R) (2017).
[63] The case where $\alpha_R < 0$ can easily be mapped into the one considered here, since the case with a $\alpha(x)$ profile can be mapped into the case $-\alpha(x)$ by space parity ($p_x \to -p_x$), as is clear from the Hamiltonian (2).

[64] E. B. Sonin, Adv. Phys. **59**, 181 (2010).
[65] E. I. Rashba, Phys. Rev. B **68**, 241315(R) (2003).
[66] J. Splettstoesser, M. Governale, and U. Zülicke, Phys. Rev. B **68**, 165341 (2003).
[67] G. Usaj and C. A. Balseiro, Europhys. Lett. **72**, 631 (2005).
[68] E. B. Sonin, Phys. Rev. B **76**, 033306 (2007).
[69] E. B. Sonin, Phys. Rev. Lett. **99**, 266602 (2007).
[70] Q.-F. Sun, X. C. Xie, and J. Wang, Phys. Rev. Lett. **98**, 196801 (2007).
[71] Q.-F. Sun, X. C. Xie, and J. Wang, Phys. Rev. B **77**, 035327 (2008).
[72] V. A. Sablikov, A. A. Sukhanov, and Y. Ya. Tkach, Phys. Rev. B **78**, 153302 (2008).
[73] F. Liang, Y. G. Shen, and Y. H. Yang, Phys. Lett. A **372**, 4634 (2008).
[74] B. Berche, C. Chatelain, and E. Medina, Eur. J. Phys. **31**, 1267 (2010).
[75] E. Nakhmedov and O. Alekperov, Phys. Rev. B **85**, 153302 (2012).
[76] H. Zhang, Z. Ma, and J. F. Liu, Sci. Rep. **4**, 6464 (2014).
[77] F. Liang, B.-L. Gao, G. Hu, Y. Gu, and N. Xu, Phys. Lett. A **379**, 3114 (2015).
[78] T.-W. Chen, C.-M. Huang, and G. Y. Guo, Phys. Rev. B **73**, 235309 (2006).
[79] F. Meier and D. Loss, Phys. Rev. Lett. **90**, 167204 (2003).
[80] I. V. Tokatly, Phys. Rev. Lett. **101**, 106601 (2008).
[81] Without magnetic field the problem Eqs. (1) and (2) can be mapped into the problem of a particle in a quantum well with a potential $E_{\rm SO}(x) = -m^*\alpha^2(x)/2\hbar^2$ by performing the spin-dependent gauge transformation $\hat{\Psi}(x) = \exp\left[im^*\sigma_z \int_0^x \alpha(x')dx'/\hbar^2\right]\hat{\Psi}'(x)$.
[82] H. A. Nilsson, Ph. Caroff, C. Thelander, M. Larsson, J. B. Wagner, L.-E. Wernersson, L. Samuelson, and H. Q. Xu, Nano Lett. **9**, 3151 (2009).
[83] S. Nadj-Perge, V. S. Pribiag, J. W. G. van den Berg, K. Zuo, S. R. Plissard, E. P. A. M. Bakkers, S. M. Frolov, and L. P. Kouwenhoven, Phys. Rev. Lett. **108**, 166801 (2012).
[84] Ö. Gü, H. Zhang, F. K. de Vries, J. van Veen, K. Zuo, V. Mourik, S. Conesa-Boj, M. P. Nowak, D. J. van Woerkom, M. Quintero-Pérez, M. C. Cassidy, A. Geresdi, S. Koelling, D. Car, S. R. Plissard, E. P. A. M. Bakkers, and L. P. Kouwenhoven, Nano Lett. **17**, 2690 (2017).
[85] P. Roulleau, T. Choi, S. Riedi, T. Heinzel, I. Shorubalko, T. Ihn, and K. Ensslin, Phys. Rev. B **81**, 155449 (2010).
[86] H. J. Joyce, C. J. Docherty, Q. Gao, H. H. Tan, C. Jagadish, J. Lloyd-Hughes, L. M. Herz, and M. B. Johnston, Nanotechnology **24**, 214006 (2013).
[87] S. Heedt, N. Traverso Ziani, F. Crépin, W. Prost, St. Trellenkamp, J. Schubert, D. Grützmacher, B. Trauzettel, and Th. Schäpers, Nat. Phys. **13**, 563 (2017).
[88] F. Romeo, R. Citro, D. Ferraro, and M. Sassetti, Phys. Rev. B **86**, 165418 (2012).
[89] P. Sternativo and F. Dolcini, Phys. Rev. B **89**, 035415 (2014).
[90] J. Strunz, J. Wiedenmann, C. Fleckenstein, L. Lunczer, W. Beugeling, V. L. Müller, P. Shekhar, N. T. Ziani, S. Shamim, J. Kleinlein, H. Buhmann, B. Trauzettel, and L. W. Molenkamp, Nat. Phys. **16**, 83 (2020).
[91] O. Krupin, G. Bihlmayer, K. Starke, S. Gorovikov, J. E. Prieto, K. Döbrich, S. Blügel, and G. Kaindl, Phys. Rev. B **71**, 201403(R) (2005).
[92] W. Wang, X. M. Li, and J. Y. Fu, J. Magn. Magn. Mater. **411**, 84 (2016).
[93] F. Nagasawa, A. A. Reynoso, J. P. Baltanás, D. Frustaglia, H. Saarikoski, and J. Nitta, Phys. Rev. B **98**, 245301 (2018).
[94] D. Rugar, R. Budakian, H. J. Mamin, and B. W. Chui, Nature (London) **430**, 329 (2004).
[95] J. Cardellino, N. Scozzaro, M. Herman, A J. Berger, C. Zhang, K. C. Fong, C. Jayaprakash, D. V. Pelekhov, and P. C. Hammel, Nat. Nanotech. **9**, 343 (2015).
[96] K. Koyke, H. Matsuyama, H. Todokoro, and K. Hayakawa, Jpn. J. Appl. Phys. **24**, 1078 (1985).
[97] T. Kohashi, J. Magn. Soc. Jpn. **39**, 131 (2015).
[98] T. Otsuka, E. Abe, Y. Iye, and S. Katsumoto, Phys. Rev. B **79**, 195313 (2009).
[99] T. Otsuka, Y. Sugihara, J. Yoneda, S. Katsumoto, and S. Tarucha, Phys. Rev B **86**, 081308(R) (2012).
[100] C. H. Li, O. M. J. van't Erve, J. T. Robinson, Y. Liu, L. Li, and B. T. Jonker, Nature Nanotech. **9**, 218 (2014).
[101] J. Tang, L.-T. Chang, X. Kou, K. Murata, E. S. Choi, M. Lang, Y. Fan, Y. Jiang, M. Montazeri, W. Jiang, Y. Wang, L. He, and K. L. Wang, Nano Lett. **14**, 5423 (2014).